

Contents list available at CBIORE journal website

# B RE International Journal of Renewable Energy Development

Journal homepage: https://ijred.cbiore.id



Research Article

# Removal of sulphur and nitrogen compounds from model fuel by adsorption of modified activated carbon

Collin Glen Joseph<sup>a,b</sup>

Narrisma Wengda Selvam<sup>c,d</sup>, S M Anisuzzaman<sup>c,d\*</sup>

- <sup>a</sup> Sonophotochemistry Research Group, Faculty of Science and Natural Resources, Universiti Malaysia Sabah (UMS), 88400 Kota Kinabalu, Sabah, Malaysia
- bIndustrial Chemistry Programme, Faculty of Science and Natural Resources, Universiti Malaysia Sabah (UMS), 88400 Kota Kinabalu, Sabah, Malaysia
- <sup>c</sup>Energy and Materials Research Group, Faculty of Engineering, Universiti Malaysia Sabah (UMS), 88400 Kota Kinabalu, Sabah, Malaysia

Abstract. This study aimed to achieve the highest percentage removal of dibenzothiophene (DBT), quinoline (QUI), and indole (IND) adsorbed by double-impregnated modified activated carbon (MAC). Modification of commercial activated carbon (AC) by sulphuric acid (H<sub>2</sub>SO<sub>4</sub>) of 15%, 30%, 45%, 60%, and 75% w/v followed by subsequent 1 zinc chloride (ZnCl2): 1 AC impregnation ratio and activated at 500 °C in a muffle furnace under self-generated atmosphere for an hour. The determination of optimized MAC was identified through the highest removal rate of DBT, QUI, and IND from adsorption experiments which were analysed using an ultraviolet-visible (UV-Vis) spectrophotometer. It was found that DBT and IND showed a removal high percentage of up to 86.23% and 82.77% respectively by using 75% H2SO4 with ZnCl2 MAC. Meanwhile, QUI favoured 30% H2SO4 with ZnCl2 MAC with a removal percentage of 33.17% which was still higher than unmodified AC. Physical and chemical properties such as the morphological structure, elemental analysis, porosity, pore size, surface functional group, percentage yield, pH, bulk density, content, ash content, and iodine number were studied for the optimized MAC. Scanning electron microscopy (SEM) and energy dispersive X-ray (EDX) spectroscopy and Fourier transform infrared spectroscopy (FTIR) were used to characterize the MAC. Both MACs showed high percentage yields of 72.08% and 71.13% for 30% and 75% H2SO4 and ZnCl2 MAC respectively. Meanwhile, the pH was between the ranges of 5.36-5.53 for both MACs. Bulk densities were also favourable while the moisture and ash content were within acceptable limits. Iodine numbers for 30% and 75% H2SO4 and ZnCl2 MAC were 857 and 861 mg/g respectively, hence indicating that the MAC achieved high porosity and good adsorption performance. Langmuir, Freundlich, and Temkin adsorption isotherm models as well as pseudo-first order (PFO) and pseudo-second order (PSO) kinetic models were considered for understanding the adsorption mechanisms. The study revealed that DBT, QUI, and IND removal processes, followed the Langmuir adsorption isotherm model with correlation coefficients, R2 of 0.9905, 0.9791, and 0.9964 respectively. Moreover, the adsorption kinetic data of DBT, QUI, and IND provided a better fitting to the PSO kinetic model with R2 of 0.9992, 0.9987, and 0.9998 respectively. According to the Langmuir isotherm model and PSO kinetic model, the adsorption mechanisms of DBT QUI and IND were chemisorbed under monolayer formations.

Keywords: sulphur-containing compounds; nitrogen containing compounds; activated carbon; desulfurization; denitrogenation; adsorption



@ The author(s). Published by CBIORE. This is an open-access article under the CC BY-SA license. (http://creativecommons.org/licenses/by-sa/4.0/). Received: 16<sup>th</sup> January 2024; Revised: 8<sup>th</sup> April 2024; Accepted: 15<sup>th</sup> June 2024; Available online: 5<sup>th</sup> August 2024

# 1. Introduction

Fossil fuels are valuable due to their efficiency in generating for transportation, power, and particularly manufacturing industries. There are traces amounts of nitrogen present in crude oil naturally but are often regarded as important quantities. Conversely, the amount of sulphur in crude oil is one of the highest atomic constituents present in crude oil. Sulphur-containing compounds (SCC) and nitrogencontaining compounds (NCC) are considered impurities that must be removed due to their detrimental impacts on the environment during crude oil processing and upon combustion of gasoline and diesel oil (Srivastava, 2012). Examples of some SCC in crude oil and coal include hydrogen sulphide, benzothiophene (BT), dibenzothiophene (DBT) and 4,6dimethyl dibenzothiophene (4,6-DMDBT) whereas examples of NCC are quinoline (QUI), indole (IND) and carbazole (CAR) (Lee et al., 2002; Mühlen et al., 2010). SCC and NCC emissions in the atmosphere are converted into acidifying chemicals such as sulphuric and nitric acid upon combustion. When these chemicals reach the ground, soil, and water, acidity arises. Soil acidity is a major contributor to danger in acidification of aquatic ecosystems and forest destruction which may endanger the lives of plant and animal species. Besides that, nitrogen oxides (NOx) also contribute to ground-level ozone depletion and eutrophication while sulphur oxides (SOx) cause adverse health effects to human beings such as lung cancer and eye irritation. The combination of SO2 and NO2 is also one of the smog and acid rain pollutants.

In the present day, catalytic hydrodesulfurization (HDS) and hydrodenitrogenation (HDN) are the typical approaches used in petroleum refining processes to reduce the sulphur and nitrogen contents in fuel. The challenges in terms of efficiency

<sup>&</sup>lt;sup>d</sup>Chemical Engineering Programme, Faculty of Engineering, Universiti Malaysia Sabah, 88400 Kota Kinabalu, Sabah, Malaysia

Corresponding author Email: anis\_zaman@ums.edu.my (S. M. Anisuzzaman)

arise for the conventional HDS technology due to its ability to remove only aliphatic sulphur compounds instead of heterocyclic aromatic sulfur compounds such as DBT and its derivatives which make up more than a fourth of the total sulphur content in fuel oil (Srivastava, 2012). Not only that, before ultra-deep desulfurization using HDS technology, NCCs should be eliminated from the fuels because they interfere with catalytic reactions by competing with SCCs for active sites thus lowering the activity of the catalysts (Almarri et al., 2009). In comparison with the HDS approach, HDN technology is relatively slow in terms of the rate of chemical reaction. In addition, the HDN technique requires the availability of hydrogen gas at relatively high temperatures and pressure which increases the production cost at a large scale. Traditional methods for pollutant removal, such as HDS and HDN, are regarded as uneconomical due to their high cost and numerous constraints and downsides.

Advancement of technologies has led to alternative techniques to remove SCCs and NCCs from model fuel such as oxidation, extraction, and bio-desulfurization. Another type of approach that has been garnering attention for its many advantages is the adsorption method. However, biodesulfurization is not sustainable in the long run due to the low activity of biocatalysts. On the other hand, extraction using ionic liquid is expensive and can sometimes contribute to environmental issues. The oxidation technique is relatively expensive for large-scale commercial stages. Adsorption is one of the most promising approaches for ultra-deep desulfurization and denitrogenation to produce cleaner fuel. Along with its low energy consumption, ability to execute at ambient temperature and pressure without the need for high-pressure hydrogen gas, ability to regenerate the spent adsorbent, and widely available, adsorptive desulfurization and denitrogenation is extensively recognized as an efficient and cost-effective way to remove organosulfur and organonitrogen compounds from model fuel (Almarri et al., 2009; Wang & Yang, 2007)

Commercial activated carbon (AC) is historically used for the adsorption of pollutants in liquid and gas phases. According to Almarri et al. (2009), AC had achieved better adsorption capacity for NCC in model diesel fuel as compared to aluminabased adsorbents. Many published studies have found a way to enhance the adsorption ability of AC through physical or chemical activation (Oliveira et al., 2019; Wu & Chen, 2008; Dehghan & Anbia, 2017; Tan et al., 2017). On the other hand, modifying AC through chemical treatment using an impregnation method can enhance surface adsorption capacity, therefore improving the efficiency of the AC to retain atoms of impurities. Adsorption capacities of DBT in model fuel doubled using prepared modified activated carbon (MAC) with Ag nanoparticles as compared to unmodified AC (Olajire et al., 2017). According to Ahmed et al. (2013), metal-organic framework (MOF) MIL-101 impregnated with phosphotungstic acid (PWA) has led to an improvement in the adsorption capacity of adsorbent to remove BT, QUI, and IND. MAC oxidized with sulphuric acid (H2SO4) at a large range of concentration has been proven to increase the removal of NCCs from model fuel (Anisuzzaman et al., 2021).

Since DBT, QUI, and IND are organic compounds, they have electron clouds and non-bound electron pairs in their atoms which exhibit high nucleophilicity. As a result, AC with acidic properties has a higher capacity to adsorb the SCC and NCC (Lopes *et al.*, 2016). In addition to that, acid pre-treated followed by metal impregnation can improve the distribution of functional groups on the surface of adsorbents (Tsai *et al.*, 2017). Dehydrating agents such as zinc chloride (ZnCl<sub>2</sub>) have been widely studied by researchers as an effective impregnation agent. It was reported by Angin (2014), that chloride is an active

agent that enhances ACs specific surface area, hence promoting higher adsorption capacity and performance. However, to date, there are insufficient studies on the effect of adsorption capacity in model fuel using MAC through double surface modification, especially via  $\rm H_2SO_4$  treatment followed by  $\rm ZnCl_2$  impregnation for removal of DBT, QUI, and IND in model fuel. In addition, there is also a need to look into the adsorption behavior of MAC in varied  $\rm H_2SO_4$  medium concentrations to compare with unmodified AC. Furthermore, this study concentrates on adsorption isotherms and kinetics to comprehend the adsorptive capabilities and mechanism of this MAC and compare it to other findings.

#### 2. Materials and Methods

### 2.1 Materials

Charcoal AC (DARCO) was purchased from Sigma-Aldrich. The charcoal AC is in granular form with mesh particle sizes ranging from 20 to 40. The charcoal AC has a total surface area of 650 m²/g, ash content of ≤0.40% as well as a moisture content of ≤12%. The sulfur-based adsorbates which are DBT (purity 98%) and nitrogen-based adsorbates which are QUI (purity, 99%) and IND (purity, 99%) were purchased from Rinitek Sdn Bhd. Malaysia. The model fuel used was n-hexane ( $C_4H_{14}$ ) with purity of 99% and also purchased from Rinitek Sdn Bhd. Malaysia. For surface modification of AC,  $H_2SO_4$  of (95 -98% purity) and  $ZnCl_2$  were also purchased from Rinitek Sdn Bhd. Malaysia.

### 2.2 Purification step of AC

The charcoal AC was immersed in hot distilled water for 2 hours and washed several times with cold distilled water to remove impurities as an additional purification step while the other chemicals were used as it is. After that, the charcoal AC was dried in a 120°C oven for 24 hours for complete drying and cooled in a desiccator afterward (Tsai *et al.*, 2017).

# 2.3 H<sub>2</sub>SO<sub>4</sub> chemical treatment followed by metal impregnation using ZnCl<sub>2</sub>

There are two modification steps of charcoal AC which is by various concentrations of H2SO4 followed by subsequent ZnCl2 impregnation. The chemical treatment method was adopted from Tsai et al., 2017 with minor modifications. Firstly, 10 g of the charcoal AC was pre-treated with 30 mL H<sub>2</sub>SO<sub>4</sub> of 15%, 30%, 45%, 60% and 75% w/v in 100 mL beakers respectively. Then, the beakers were sealed with aluminium foil with punched holes to allow vapor evaporation. In order to allow for thorough dissolution, the beakers were then kept in the sonicator bath for three days. The H<sub>2</sub>SO<sub>4</sub>-treated AC was filtered with filter paper and washed with distilled water before it was dried in a 120°C oven for 24 hours to remove excess moisture. The subsequent ZnCl<sub>2</sub> impregnation procedures were referred from Angin (2014) and Yakub et al., (2013). ZnCl2 solution was prepared by solubilizing 10.0 g of ZnCl2 solids in 250 mL distilled water. 15% H<sub>2</sub>SO<sub>4</sub>-treated AC was transferred into the beaker containing ZnCl<sub>2</sub> solution for (1 ZnCl<sub>2</sub>:1 H<sub>2</sub>SO<sub>4</sub>-treated AC) impregnation. The flask was left to shake at 80°C for 24 hours for a complete reaction. After this, the samples were filtered using filter paper and left to dry at 120°C oven for 24 hours to remove excess zinc and chlorine. The impregnation with ZnCl2 was repeated for 30%, 45%, 60%, and 75% w/v  $H_2SO_4$ . The samples were then weighed using an analytical balance to record the final mass of AC obtained before it was activated in a muffle furnace under self-generated atmosphere conditions at 500°C for an hour. After reaching room temperature, the AC was rinsed with 1M

potassium hydroxide (KOH) solution to remove possible clogs of zinc and chloride from the pores of the AC and neutralize pH of the AC. Distilled water was used to rinse the MAC until the pH reached neutral at 6-7. Finally, the prepared MAC was dried in a 120°C oven for 24 hours before storing in a glass bottle for characterization tests.

### 2.4 Preparation of DBT, OUI and IND stock solution

Stock solution for DBT, QUI and IND of 1000 mg/L each was prepared by dissolving 1000 mg of the adsorbates in 1 l n-hexane solution. A standard calibration curve of DBT, QUI, and IND were plotted where y-axis and x-axis represents absorbance value and adsorbate concentration respectively. DBT, QUI and IND were then diluted to 20 mg/L, 40 mg/L, 60 mg/L, 80 mg/L, and 100 mg/L using dilution Equation (1):

$$M_1 V_1 = M_2 V_2 \tag{1}$$

where,  $M_1$  is Initial molarity (mg/L);  $V_1$  Initial volume (L);  $M_2$  Final molarity (mg/L);  $V_2$  = Final volume (L)

## 2.5 Adsorption experiment for determination of best MAC

100 mL n-hexane fuel solutions of DBT, QUI, and IND were prepared by placing them in three separate beakers with an initial concentration of 100 mg/L each. Next, 1g of ZnCl2impregnated MAC that was pre-treated with 15% H2SO4 solution was added to each beaker. Then, beakers were magnetically stirred at 160 rpm for 1 hour in an isothermal water bath at room temperature. After 1 h of stirring, solid residues were separated with filter paper, and the filtered solution was analysed using ultraviolet-visible (UV-Vis) spectrophotometry at maximum wavelength of DBT, QUI and IND. The experiment was repeated using ZnCl2-impregnated MAC with 30%, 45%, 60%, and 75% pre-treated H<sub>2</sub>SO<sub>4</sub> and unmodified AC. The final unknown concentration of DBT, QUI, and IND in n-hexane with an initial concentration of 100 mg/L each was determined from the standard calibration curve of each of the adsorbates. Then, the percentage removal of DBT, QUI, and IND from n-hexane by modified and unmodified AC was calculated according to Equation (2):

$$\% Removal = \frac{(C_o - C_t)}{C_o} \times 100$$
 (2)

where,  $C_o$  is Initial adsorbate concentration (mg/L);  $C_t$  Adsorbate concentration at a given time (mg/L).

## 2.6 Characterization of best MAC

# 2.6.1~% yield determination

The % yield was calculated by weighing 30% and 75%  $H_2SO_4$  and  $ZnCl_2$  impregnated MAC which was then divided by the initial weight of AC before modification which is expressed in Equation (3)

Yield, 
$$\% = \frac{Final\ weight\ of\ MAC\ (g)}{Initial\ weight\ of\ AC\ (g)} \times 100$$
 (3)

## 2.6.2 pH determination

1.0~g of 30% and  $75\%~H_2SO_4$  and  $ZnCl_2$  impregnated MAC was weighed and placed in a beaker and 100 mL distilled water was added. Then, the beaker was heated to a temperature of  $40^{\circ}C$  and left to cool down to room temperature once the thermometer temperature hits  $40^{\circ}C$ . The pH value was determined by using a Mettler Toledo pH meter.

#### 2.6.3 Bulk density determination

The bulk density of MAC method was determined by Efeovbokhan *et al.*, 2019. Firstly, 25 mL measuring cylinder was placed on analytical balance and tare. The MAC was then poured into the measuring cylinder until it reached the 25 mL marking. To prevent voids, the measuring cylinder was tapped. The weight shown on the analytical balance was recorded and bulk density was calculated according to Equation (4):

$$Bulk \ density = \frac{Mass \ of \ MAC \ (g)}{Volume \ of \ measuring \ cylinder \ (mL)} \tag{4}$$

#### 2.6.4 Moisture content determination

The moisture content in MAC was determined from a procedure done by Jeyakumar & Chandrasekaran, 2014. 1.0 g of MAC was dried at 110°C in an oven for 3 h and cooled in a desiccator before weighing. The process of heating, cooling, and weighing was repeated until a constant mass of MAC was achieved. The calculation for moisture content is expressed in Equation (5) (Jeyakumar & Chandrasekaran, 2014).

Moisture content, 
$$\% = \frac{100 \times (M-X)}{M}$$
 (5)

where, M is mass in gram of the sample taken for the test, X mass in gram of the sample after drying

### 2.6.5 Ash content determination

The determination of ash content was done by weighing MAC right after moisture content test in a muffle furnace of 500°C for 4 hours. Then, the ash was cooled in desiccator before reweighing. Ash content was calculated using Equation (6) (Jeyakumar & Chandrasekaran, 2014).

Ash content, 
$$\% = \frac{M_1 x 100}{M x (100 - X)/100}$$
 (6)

where,  $M_1$  is mass of ash in grams, M mass of the sample taken for the test in gram, X percentage of moisture content present in the sample taken for the test.

# 2.6.6 Iodine number determination

The iodine number was determined according to the standard ASTM D460794 method. Firstly, 1 g of MAC was mixed with 10 mL of 5% HCl solution and boiled for 30 seconds before allowing cooling. Then, 100 mL of 0.1N iodine solution was poured into the conical flask and stirred vigorously for 30 seconds before filtering with filter paper. 50 mL of the filtrate was titrated against 0.1N sodium thiosulphate solution until the solution turned pale yellow. Once the pale yellow was formed, 2 mL of starch solution was added to the conical flask. When the solution turned colourless, titration was stopped, and the amount of sodium thiosulphate utilized was recorded. Two important calculations were required which are shown in Equations 7 and 8. Equation 7 presents the amount of iodine adsorbed for 1.0 g of MAC while Equation 8 is the concentration of iodine in the filtered solution.

X/M presents the amount of iodine adsorbed for 1 g of MAC while C is the concentration of iodine in the filtered solution.

$$\frac{X}{M} = \frac{A - (DF \times B \times S)}{M} \tag{7}$$

where, A = 12693 (used sodium thiosulphate (mL)  $\times$  0.1)/100 ml, DF = (100+10) ml/50 ml = 2.2, B = 0.1N(126.93), S = used sodium thiosulphate (mL), M is MAC dosage

$$C = \frac{0.1 \times S}{F} \tag{8}$$

where, S is used sodium thiosulphate (ml); F Filtrate used (50 mL)

Then a graph of X/M against C was plotted for another two different dosages (2 g and 3 g). At C = 0.02 N on the plot, the iodine number was determined from X/M.

# 2.6.7 Functional group determination using fourier transform infrared spectroscopy (FTIR)

The functional groups and covalent bonding present in the 30% and 75% H<sub>2</sub>SO<sub>4</sub> + ZnCl<sub>2</sub> MAC as well as unmodified AC were analysed and compared using a FTIR model Inveio-R Bruker with the wavenumber range set between 400 to 4000 cm<sup>-1</sup>. This effective analytical instrument was able to identify the MAC surface functional groups which participated in the adsorption capability of MAC to to form temporary bonds with DBT, QUI and IND from n-hexane.

# 2.6.8 Scanning electron microscopy (SEM) and energy dispersive X-ray (EDX) spectroscopy analysis

The surface morphology and topography such as pore shape, pore distribution, and pore size of the MAC and unmodified AC were visualized using a scanning electron microscope with energy dispersive X-ray (SEM-EDX) model Hitachi. The direct microstructure changes on the surface of the MAC were observed using SEM and comparisons were made with the unmodified CAC. The magnifications were adjusted from 100x to 3000x to obtain a high-resolution image. On the other hand, the EDX results were used to determine the type and amount of each element present in both types of CAC. Sample preparation for both the 30% and 75% H<sub>2</sub>SO<sub>4</sub> and ZnCl<sub>2</sub> MAC via gold coating was prepared using Quorum Q150T ES plus sputter coater to increase the conductivity of the samples and beam sensitivity.

## 2.6.9 Surface morphology analysis

A Java-based image processing program called *ImageJ* was used to analyze the surface morphology such as pore size and porosity of the 30% and 75% H<sub>2</sub>SO<sub>4</sub> + ZnCl<sub>2</sub> MAC and unmodified AC. This software was developed by researchers from the National Institutes of Health and the Laboratory for Optical and Computational Instrumentation at the University of Wisconsin. *ImageJ* program is relatively simple as it is designed to calculate distance and area and develop statistical graphs according to the results (Chilev, 2017). Hence, this software was utilized to identify the pore size and porosity of the captured modified and unmodified CAC images from SEM.

### 2.7 Adsorption isotherm and kinetic models

# 2.7.1 Determination of adsorption isotherm

Batch isotherm experiments were conducted to determine the most suitable isotherm model, i.e, Langmuir, Freundlich, or Temkin, which can explain the adsorption relationship between the unbounded and bounded DBT, QUI, and IND on MAC surface. n-hexane fuel solution with varied concentrations of DBT, QUI, and IND but with constant MAC dosage was tested. Firstly, 100 mL of model fuel solution consisting of 20 mg/L of DBT, QUI and IND was prepared in three separate beakers.

Next, 1 g of optimized MAC was added into all beakers and magnetically stirred in 25°C water bath at 160 rpm for 1 h. To separate solid residues, a filter paper was used, and the filtered solution was then analysed using UV-VIS spectrophotometry at maximum wavelength of DBT, QUI, and IND. The experiment was repeated with varying concentration which is 40 mg/L, 60 mg/L, 80 mg/L and 100 mg/L of DBT, QUI, and IND in 100 mL n-hexane fuel solution. The final unknown concentration of DBT, QUI, and IND in n-hexane that had an initial concentration of 100 mg/L each was determined from the standard calibration curve of each of the adsorbates. Then, the amount of DBT, QUI and IND at equilibrium was determined by using Equation (9).

$$Q_e = \frac{(C_o - C_e)V}{W} \tag{9}$$

where,  $Q_e$  = amount of adsorbate adsorption at equilibrium (mg/g);  $C_o$  = initial adsorbate concentration (mg/L);  $C_e$  = equilibrium adsorbate concentration (mg/L); V = Volume of solution (l); W = weight of MAC used (g)

After determining the amount of DBT, QUI and IND absorbed at equilibrium, the data was fitted to form linear graphs according to the theoretical equations of Langmuir isotherm, Freundlich isotherm and Temkin isotherm.

· Langmuir model equation:

$$\frac{C_e}{Q_e} = \frac{C_e}{Q_{max}} + \frac{1}{K_L Q_{max}} \tag{10}$$

$$R_L = \frac{1}{K_L C_O} \tag{11}$$

where,  $Q_{max}$  is maximum monolayer adsorption capacity (mg/g),  $K_L$ = Langmuir isotherm constant (mg/l),  $C_e$  equilibrium adsorbate concentration (mg/l),  $Q_e$  amount of adsorbate adsorption at equilibrium (mg/g),  $R_L$  separation factor,  $C_o$  initial adsorbate concentration (mg/L).

Freundlich model equation

$$\log Q_e = \frac{1}{n} \log C_e + \log K_F \tag{12}$$

where,  $C_e$  is equilibrium adsorbate concentration (mg/L),  $Q_e$  amount of adsorbate adsorption at equilibrium (mg/g), n adsorption intensity (mg/g),  $N_F$  Freundlich isotherm constant (mg/g).

Temkin model equation

$$Q_e = \left[\frac{RT}{b_T}\right] \ln C_e + \frac{RT}{b_T} \ln A_T \tag{13}$$

where,  $C_e$  is equilibrium adsorbate concentration (mg/L);  $b_T$  Temkin constant corresponding to enthalpy of sorption (kJ/mol),  $A_T$  Temkin binding constant at equilibrium (l/mg), R universal gas constant (kJ/mol.K), T Temperature (K),  $Q_e$  amount of adsorbate adsorption at equilibrium (mg/g).

# 2.7.2 Determination of adsorption kinetic model

In this study, n-hexane fuel solution with constant concentration DBT, QUI and IND and constant MAC dosage was performed with time intervals from 1 to 5 h. 100 mL of model fuel solution consisting of 100 mg/L of DBT, QUI and IND in three separate beakers were prepared. Next, 1 g of the optimised MAC was added into all beakers and magnetically stirred at 25°C in a water bath at 160 rpm for an hour. To separate solid residues, a filter paper was used and the filtered solution was analyzed using UV-VIS spectrophotometry at

maximum wavelength of DBT, QUI and IND. The experiment was repeated with the following mixing time of 2 to 5 h. The final unknown concentration of DBT, QUI and IND in n-hexane with initial concentration of 100 mg/L each was determined from the standard calibration curve of each of the adsorbates. Then, the amount of DBT, QUI and IND at equilibrium was determined by using adsorption using Equation (14).

$$Q_t = \frac{(c_t - c_t)V}{W} \tag{14}$$

where,  $Q_t$  = amount of adsorbate adsorption at equilibrium at given time (mg/g),  $C_t$  initial adsorbate concentration at given time (mg/L),  $C_t$  equilibrium adsorbate concentration at given time (mg/L), V volume of solution (L), W weight of MAC used (g).

After that, the data was fitted to form linear graphs according to the theoretical equations of pseudo-first order (PFO) model and pseudo-second order (PSO) model as below.

• PFO) model equation

$$\ln(Q_e - Q_t) = -K_1 t + \ln Q_e \tag{15}$$

where,  $Q_t$  is amount of adsorbate adsorption at time (mg/g),  $K_1$  PFO adsorption rate constant (hr<sup>-1</sup>), t mixing time (hr),  $Q_e$  amount of adsorb at adsorption at equilibrium (mg/g).

• PSO model equation

$$\frac{t}{Q_t} = \frac{t}{Q_e} + \frac{1}{K_2 Q_e^2} \tag{16}$$

where,  $Q_t$  is amount of adsorbate adsorption at time (mg/g),  $K_2$  PSO adsorption rate constant (g/mg.hr), t mixing time (hour);  $Q_e$  amount of adsorbate adsorption at equilibrium (mg/g)

### 3. Results and Discussion

3.1 Adsorption of DBT, QUI and IND to determine the best MAC

The optimised MAC was identified through the adsorption of DBT, QUI and IND in n-hexane using various MAC and the

results are shown in Figure 1 for each adsorbate. The final concentration was calculated from the standard calibration curve equation for the given adsorbate.

As shown in Figure 1, the optimised MAC for adsorbing DBT and IND is 75% H<sub>2</sub>SO<sub>4</sub> pre-treated AC followed by ZnCl<sub>2</sub> modification while the best MAC for adsorbing QUI is 30% H<sub>2</sub>SO<sub>4</sub> pre-treated AC followed by ZnCl<sub>2</sub> modification. Among all adsorbates, DBT showed a substantially high % removal using the MAC. This could be due to the presence of high surface acidity on MAC which favoured DBT removal over the other NCC adsorbates. Similar observations were reported by Lopes et al. (2016), who concluded that higher SCC (up to 75%) than NCC were removed especially after modification with H<sub>2</sub>SO<sub>4</sub>. This is because DBT is a sulphur base adsorbate that is attracted to more acid groups present on 75% H<sub>2</sub>SO<sub>4</sub> + ZnCl<sub>2</sub> MAC, thus it facilitates easier binding to large pores, hence better adsorption performance (Seredych et al., 2009). On the other hand, QUI favoured 30% H<sub>2</sub>SO<sub>4</sub> concentration rather than 75% H<sub>2</sub>SO<sub>4</sub> concentration because the high temperature (500°C) applied during activation, removed more carboxylic acid groups that were essential for the adsorption of OUI in 75% H<sub>2</sub>SO<sub>4</sub> + ZnCl<sub>2</sub> MAC. These findings were similarly reported by Qu et al. (2016).

### 3.2 Physiochemical characteristics of MAC

Table 1 lists the comparison of results obtained from physiochemical characterization study using 30% and 75%  $\rm H_2SO_4$  ZnCl<sub>2</sub> MAC. The % of yield for the optimised MAC was 30% and 75%  $\rm H_2SO_4$  pre-treated AC followed by ZnCl<sub>2</sub> impregnation ratio 1:1 was 72.08% and 71.13% respectively. Table 1 shows the 75%  $\rm H_2SO_4$  dosage MAC resulted in a slightly lower % yield than the 30%  $\rm H_2SO_4$  dosage. From the results, it was observed that the samples suffered a considerable mass loss. This was likely caused by AC oxidation, which degrades not only the inorganic constituents but also the organic constituents present in the AC before surface modification. According to Pratumpong & Toommee (2016), ZnCl<sub>2</sub> with an impregnation ratio of 1:1 yielded the highest waste-derived AC which is at 47.82%. Another study concluded that an increase in ZnCl<sub>2</sub> impregnation ratio could increase the % of yield of waste-

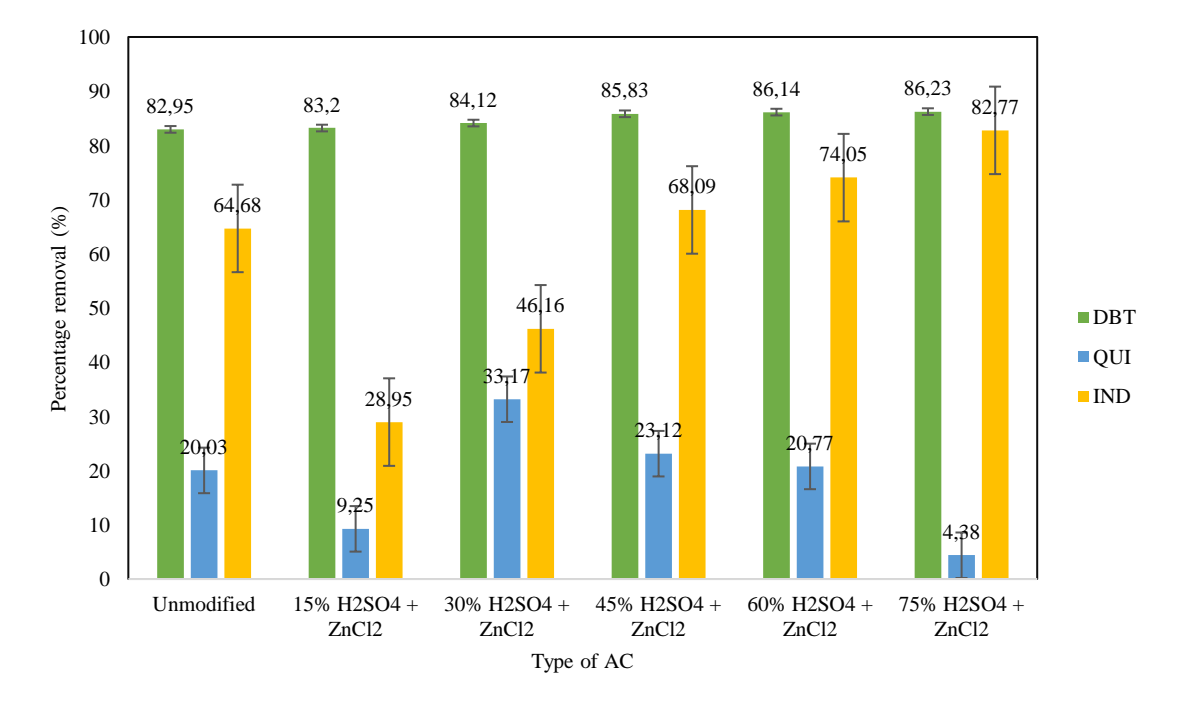


Fig 1 Percentage removal vs. type of AC for DBT, QUI and IND

G. C. Joseph et al

**Table 1**Physiochemical characterization comparison between MAC

Physiochemical study	30% H <sub>2</sub> SO <sub>4</sub> with ZnCl <sub>2</sub> MAC	75% H <sub>2</sub> SO <sub>4</sub> with ZnCl <sub>2</sub> MAC
% yield	72.08	71.13
pH	5.53	5.36
Bulk density, g/cm <sup>3</sup>	0.42	0.43
Moisture content, %	4.88	4.46
Ash content, %	3.17	2.68
Iodine number, mg/g	857	861

derived AC to 47.08% (Awe et al., 2020). However, the observed yield from this experiment was comparatively higher than those reported in the mentioned studies. This could be due to the usage of commercial AC while the ones mentioned in the studies are waste-derived AC that contains highly volatile matter that is easily burned off upon carbonization especially when oxygen and hydrogen atoms found in the carbonaceous structure, bind together, hence, forming water molecule (Bouchemal et al., 2009). Similar findings were reported by Yahya et al. (2015) who concluded that % of yield of AC prepared by coal as raw material was higher than that of wastederived AC. Chemical agents such as ZnCl2 have been studied by other researchers to boost product yield and reduce burn-off. This is because ZnCl<sub>2</sub> functions as a catalyst to accelerate dehydration which is essential for promoting cross-link bonds, thus forming a rigid matrix (Iwanow et al., 2020). Due to the hard and solid structure, the modified AC can release lower volatile compounds during carbonization, hence achieving higher AC yields. From the results, it can be said that the surface modification using H<sub>2</sub>SO<sub>4</sub> and ZnCl<sub>2</sub> can prevent the production of tar and other substances which could clog the pores of the AC during the activation process since these activating agents have the potential to conserve carbon, minimize the loss of volatile matter and open up pores due to the reduction in mass (Bouchemal et al., 2009).

One of the most important parameters that have a significant impact of the adsorption of specific compounds by is the pH of the absorbent. This is because the pH of absorbent will determine the type of surface groups on AC matrix, whether it is acidic or basic (Jeyakumar & Chandrasekaran, 2014). The surface chemistry of the AC can be altered during preparation by adding chemical activating agents (Iwanow et al., 2020). Moreover, the uptake of DBT, QUI and IND were strongly dependent of the acid sites available of the surface of the MAC (Ahmed et al., 2013). Since H<sub>2</sub>SO<sub>4</sub> and ZnCl<sub>2</sub> are acidic compounds, the typical pH range of MAC should be between 4 to 6 (Hakimi et al., 2017). In this study, the pH for 30% H<sub>2</sub>SO<sub>4</sub> pre-treated and ZnCl<sub>2</sub> MAC was found to be 5.53 while the pH for 75% H<sub>2</sub>SO<sub>4</sub> pre-treated and ZnCl<sub>2</sub> MAC was 5.36, hence proving that the modified AC is slightly acidic. According to Lopes et al. (2016), the modification of AC using H<sub>2</sub>SO<sub>4</sub> absorbed the high percentage of sulphur and nitrogen from commercial diesel as compared with nitric acid and hydrochloric acid due to its presence of highest number of oxygen-containing functional groups on the surface of AC which are also known as acidic groups. Another study conducted by Ahmed et al., (2013), confirmed that acidic conditions favoured adsorption of DBT, QUI and IND. The reason to it is because DBT and QUI are hard and soft base adsorbates respectively while IND is a neutral adsorbate. Acid-modified AC improved adsorptive performance of DBT and QUI due to its strong acid-base interactions. Similarly, it was also reported by (Sarker et al., 2018), that adsorption performance of QUI and IND increased linearly with an increase in oxygenated functional groups on the absorbent.

The bulk density of a prepared AC is an important parameter in determining its suitability for specific applications.

AC with low bulk density shows that less AC is required to be filled into a given space while higher bulk densities require higher AC volume to fit into the given space. Therefore, higher bulk density carbon would result in a better adsorption performance of adsorbate as compared to low density carbon. The bulk density of raw AC was determined to be 0.38 g/cm<sup>3</sup> whereas, with double impregnation of 30% H<sub>2</sub>SO<sub>4</sub> and ZnCl<sub>2</sub>, the bulk density increased slightly to 0.42 g/cm<sup>3</sup>. The bulk density further increased to 0.43 g/cm³ with 75% H<sub>2</sub>SO<sub>4</sub> and ZnCl<sub>2</sub> treatment. Based on study by Efeovbokhan et al. (2019), the bulk density of AC is dependent on the activation chemical and carbonization temperature where, lower activation temperature with bio-acid activators increased bulk density of AC, indicating that adsorption capabilities were better than of bio-base activators with high carbonization temperature. This is in agreement with Yusufu et al., (2012), which concluded that acid activation treatment can significantly increase the bulk densities of AC up to 18% for wood precursor AC. The increment of ZnCl2 concentration as an activating agent had reported a higher bulk density due to the expansion of molecules which resulted from the cross-linking reaction (Akpa et al., 2018).

Moisture content can be defined as the amount of water that is physically retained in the AC sample under standard conditions. The amount of moisture present in the AC of the 30% and 75% H<sub>2</sub>SO<sub>4</sub> pre-treated AC followed by ZnCl<sub>2</sub> impregnation are 4.88% and 4.46% respectively. The 75% H<sub>2</sub>SO<sub>4</sub> pre-treated AC followed by ZnCl<sub>2</sub> has lower moisture content because of the higher concentration of H2SO4 used which promotes better dehydrating effect (Akpa et al., 2018). Similar results were obtained by Owabor & Iyaomolere (2013), which also reported that increasing concentration of activating agent had decreased the moisture content in the AC due to higher dehydration rate but only until a certain limit until concentration had no influence on the moisture content. Moreover, higher acid concentration is advantageous for enhancing the surface area of AC, and thus decreasing the AC's hygroscopic characteristics (Suhdi & Wang, 2021). Lower moisture content would contribute to higher percentage yield (Efeovbokhan et al., 2019). The adsorption performance of adsorbate onto MAC is affected by the moisture content because higher moisture content would mean that more water molecules were occupying the micropores of AC, inhibiting and competing with adsorbate molecules to potentially occupy those active sites during adsorption process. Zhou et al. (2001) observed that higher moisture content showed a negative trend on the adsorption performance, thus lowering the efficiency of AC.

Ash content is one of the physiochemical characteristics that determine the quality of the modified AC. Ash content is the inorganic and unstable fraction of AC that does not chemically react with any components such as calcium, magnesium, and silica that remain after carbonization (Jeyakumar & Chandrasekaran, 2014). The ash content of AC varies from one to another depending on the mineral compounds that are available in the precursor raw material

(Iwanow et al., 2020). Generally, the ash content of an AC after chemical activation ranges from 1% to 20% depending on the type of starting material (Zulkania et al., 2018). The presence of a high ash content percentage is undesirable during AC preparation because it influences the adsorption performance due to the reduction in carbon mechanical strength (Zulkania et al., 2018). In addition to that, the purity of the carbon is reflected in the ash level which also impacts the adsorption performance by creating inactive sites and clogged pores (Martínez-Mendoza et al., 2020; Yusufu, et al., 2012). The ash content of the 30% and 75% H<sub>2</sub>SO<sub>4</sub> pre-treated AC followed by ZnCl<sub>2</sub> impregnation are 3.17% and 2.68% respectively. These values are significantly higher than ash content present in commercial AC which is ≤0.40%. This indicates that ash content increased with the double impregnation using H<sub>2</sub>SO<sub>4</sub> and ZnCl<sub>2</sub>. This result could be attributed to the presence of remaining activating agent residuals and insoluble organic compounds entrapped in the ash along with AC (Yusufu et al., 2012). However, the 75% H<sub>2</sub>SO<sub>4</sub> pre-treated AC with ZnCl2 modification has a lower ash content due to the reaction of acid with mineral components in the AC as well as low char burn-off, hence contributing to lower ash content (Owabor & Iyaomolere, 2013; Yusufu et al., 2012). The results of ash content in this study are significantly lower than compared to previous research studies of Owabor & Iyaomolere (2013) and Dagde (2018) in which impregnation ratio of 1:1 ZnCl<sub>2</sub> reported 4.72% and 7.80% ash content respectively. Another study by Mkungunugwa et al. (2021), observed that activation using higher H2SO4 concentration reduced the ash content of AC from 3.49% to 0.97% using 40% and 60% H<sub>2</sub>SO<sub>4</sub> concentration respectively.

Iodine number also known as iodine index is another crucial characterization analysis that is defined as the mass of iodine that is adsorbed by a certain weight of MAC (on a dry basis) at an equilibrium concentration. It also provides information on the degree of porosity of the MAC. According to Jeyakumar & Chandrasekaran (2014), a higher iodine number represents a higher activation stage. Since the results are plotted on logarithmic axes, where the corresponding iodine number can be found when residual filtrate normality is 0.02 according to the ASTM-D4607, hence it is only a rough estimate of the micropore surface area of MAC. The estimated iodine number for 30% and 75%  $H_2SO_4$  ZnCl<sub>2</sub> MAC are 857 mg/g and 861 mg/g respectively. The iodine number of both MAC is within

the typical range of 500-1200 mg/g (Mopoung *et al.*, 2015). The iodine number results were expected to increase for 75%  $\rm H_2SO_4$   $\rm ZnCl_2$  MAC since a higher  $\rm H_2SO_4$  concentrations were used for the surface modification process. Besides that, the results indicate that the 75%  $\rm H_2SO_4$   $\rm ZnCl_2$  MAC has a more accessible micropore volume and large surface area as compared to the 30%  $\rm H_2SO_4$   $\rm ZnCl_2$  MAC due to a slightly higher iodine number. Similarly, Yusufu *et al.* (2012) reported that the iodine number increased concerning concentration of acid utilized for surface modification of AC. In addition to that, a high iodine number for both modified AC promotes higher pore development and it corresponds with the adsorption performance of DBT, QUI, and IND from n-hexane.

### 3.3 FTIR analysis

AC is typically made up of carbon atoms, but it also contains different heteroatoms such as hydrogen, oxygen, nitrogen, and sulphur (Iwanow *et al.*, 2020). The surface functional groups and other chemical component structures contained in AC were identified using FTIR analysis, which is significant in characterizing and predicting adsorption performance (Mkungunugwa *et al.*, 2021). The spectra were recorded between the range of 4000 cm<sup>-1</sup> and 400 cm<sup>-1</sup>. The samples' spectra revealed the existence of various active functional groups which demonstrates a decrease, emergence, disappearance, or widening of the peaks following the impregnation procedure with 30% and 75% H<sub>2</sub>SO<sub>4</sub> pre-treated AC followed by ZnCl<sub>2</sub> impregnation.

The FTIR spectra of 30% and 75%  $H_2SO_4$  pre-treated AC followed by  $ZnCl_2$  impregnation showed considerably more functional groups present of the surface of MAC as compared to unmodified AC (Figure 2). It can be observed that the rise of two bandwidths between 690 cm<sup>-1</sup> to 600 cm<sup>-1</sup> and 1130 cm<sup>-1</sup> to 1090 cm<sup>-1</sup> in all FTIR spectra corresponds to S=O and S-O stretching with indication that there is presence of sulphate ion even before  $H_2SO_4$  and  $ZnCl_2$  modification . However, the peaks around 690 cm<sup>-1</sup> to 600 cm<sup>-1</sup> were stronger for 30% and 75%  $H_2SO_4$  pre-treated AC and  $ZnCl_2$  as compared to unmodified AC because of the high  $H_2SO_4$  concentration used during the modification process. Another common peak for C=C weak stretching found in aromatic rings which is around 1600 cm<sup>-1</sup> to 1510 cm<sup>-1</sup>. This is because of the tars formed from aromatization

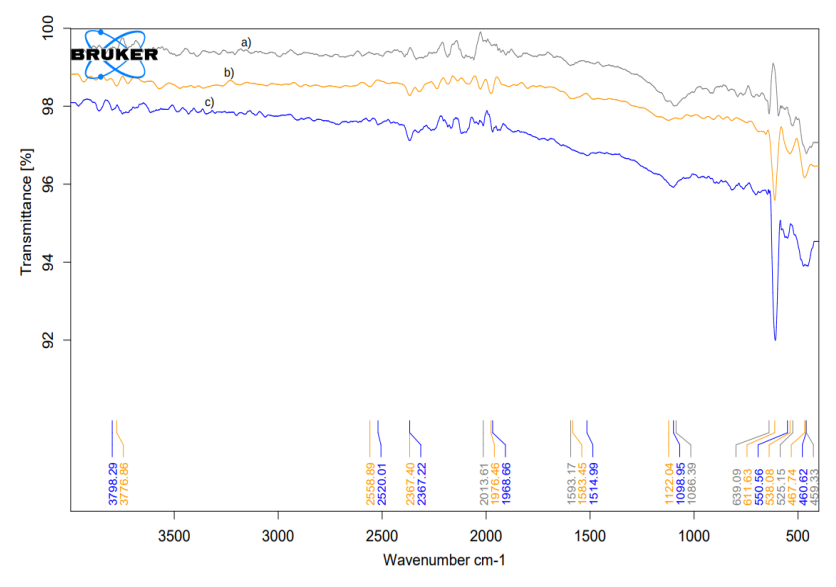


Fig 2 FTIR spectra for a) unmodified AC, b) 75% H<sub>2</sub>SO<sub>4</sub> pre-treated AC + ZnCl<sub>2</sub> impregnation c) 30% H<sub>2</sub>SO<sub>4</sub> pre-treated AC + ZnCl<sub>2</sub> impregnation

and decomposition of C-H bonds, followed by condensation and dehydration hence, influencing formation of aromatic compounds with cross linking to generate more stable aromatic bond (Mopoung et al., 2015). The bandwidths between 2400 cm-<sup>1</sup> and 1900 cm<sup>-1</sup> were noted to be substantially stronger at 30% and 75% H<sub>2</sub>SO<sub>4</sub> pre-treated AC and ZnCl<sub>2</sub> as compared to unmodified AC due to asymmetric or symmetric stretching in aliphatic band in -CH, -CH<sub>2</sub> or -CH<sub>3</sub>. The increase in aliphatic structure is possibly caused by the extraction of OH and H functional groups from aromatic rings during the double impregnation as well as the dehydrating effect of ZnCl2 (Angin, 2014). Besides that, the presence of aliphatic group indicates that they are organic compounds which contain carbonhydrogen bond that is able to bind to other elements including but not limited to sulphur, nitrogen, oxygen and chlorine adsorbates (Mkungunugwa et al., 2021). The difference between unmodified AC and MAC is the presence of S-H weak stretching representing thiol compound, found between bandwidth range of 2600 cm $^{\text{-}1}$  to 2500 cm $^{\text{-}1}$  only for 30% and 75%  $H_2SO_4$  pretreated AC and ZnCl2 modified AC (Lesaoana et al., 2019). Therefore, this proves that the sulphur was successfully incorporated to form thiol compound on the surface of MAC. In addition to that, the peak observed between bandwidth of 3800 cm<sup>-1</sup> to 3500 cm<sup>-1</sup> represents O-H stretching, indicating the presence of intermolecular bonded hydroxyl functional groups such as carboxylic acid which could be the result of H2SO4 surface modification, thus generating more acidic functional groups on AC surface while reducing hydroxide functional groups (Jawad et al., 2016).

## 3.4 SEM-EDX analysis of MAC

The study for the morphological structure and elemental composition in unmodified and MAC was carried out using the SEM-EDX analysis. The SEM images were observed at the magnification of 1000x for all samples. The images of each sample before and after modification are shown in Fig . As shown in Fig (a), the surface area of unmodified AC is smoother, and the pores are not as visible as in 30% and 75% H<sub>2</sub>SO<sub>4</sub> + ZnCl<sub>2</sub> MAC. The surface of the unmodified shows some pores scattered however, there are no visible cracks. In contrast, the surface of 30% and 75% H<sub>2</sub>SO<sub>4</sub> + ZnCl<sub>2</sub> MAC which are shown in Fig (b) and 3(c) respectively has a more defined pore development at various shapes and sizes. This is attributed to the dehydrating effect of ZnCl<sub>2</sub> during the activation process that leaves spaces previously occupied by ZnCl2, thus producing more cavities on the AC's surface (Angin, 2014). The higher the number of visible pores present on the surface of AC, the better possibility of DBT, QUI, and IND adsorption by AC. The high activation temperature coupled with thermal stress forms fissures, crevices, cracks, and slits leading to pore formation (Achaw, 2012). Besides that, the introduction of a strong acid like H<sub>2</sub>SO<sub>4</sub> creates significantly defined pores that are favourable for the adsorption process (Mahmud et al., 2018). The modification of AC with H2SO4 followed by ZnCl2 forms significant and consistent pores that are well-structured on the AC's surface, indicating that both of the MAC have a more porous surface than the unmodified AC. According to Angin, 2014, the usage of ZnCl<sub>2</sub> formed AC full of cavities and high surface area as compared to unmodified AC.

The EDX analysis was conducted to identify differences in elemental composition between MAC and unmodified AC. The analysis was taken from specific points from the SEM images of unmodified, 30% and 75%  $\rm H_2SO_4$  +  $\rm ZnCl_2$  MAC which are presented in Figure 4a,b and c, respectively. In all samples, gold (Au) was detected owing to the fact that all samples were gold coated for SEM analysis. The presence of sodium (Na), iron (Fe), and rhenium (Re) were only found in 30% and 75%  $\rm H_2SO_4$  +  $\rm ZnCl_2$  MAC due to the corrosive nature of  $\rm H_2SO_4$  especially at high temperatures during drying which caused thinning of the

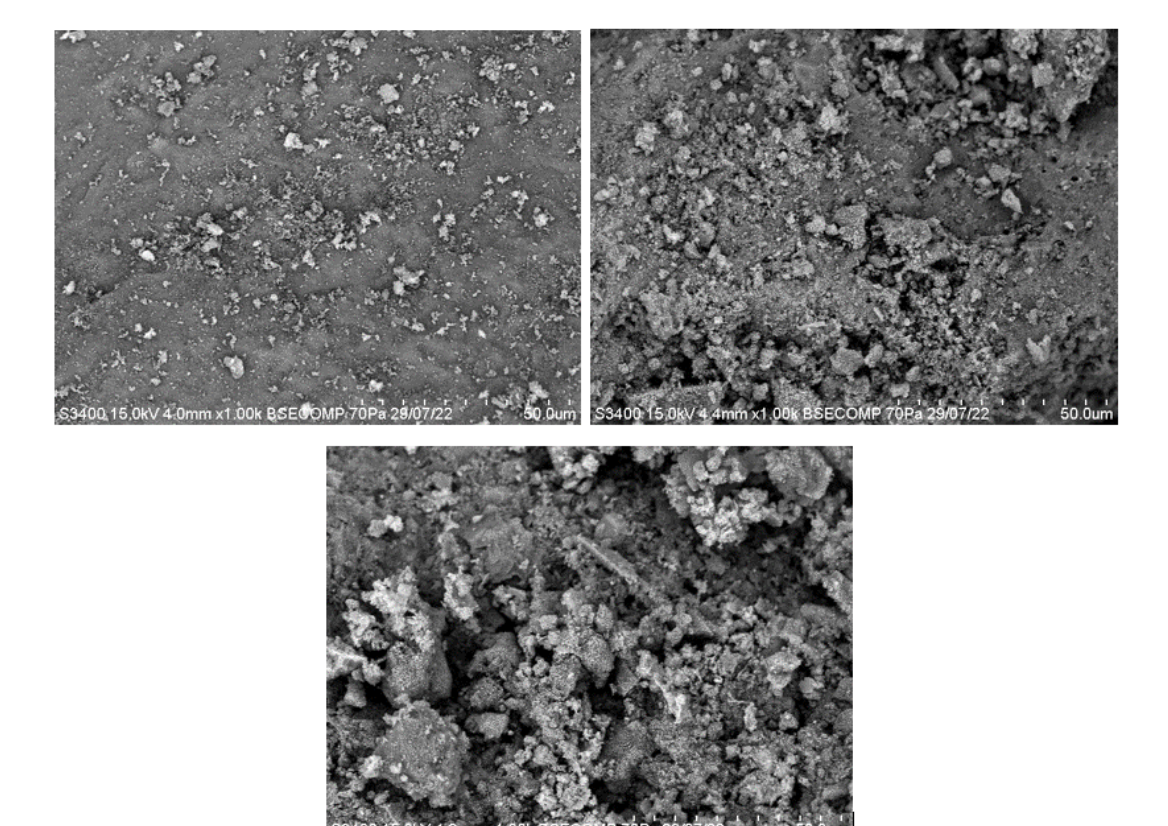


Fig 3 SEM images for a) unmodified AC, b) 30% H<sub>2</sub>SO<sub>4</sub> + ZnCl<sub>2</sub> MAC, c) 75% H<sub>2</sub>SO<sub>4</sub> + ZnCl<sub>2</sub> MAC

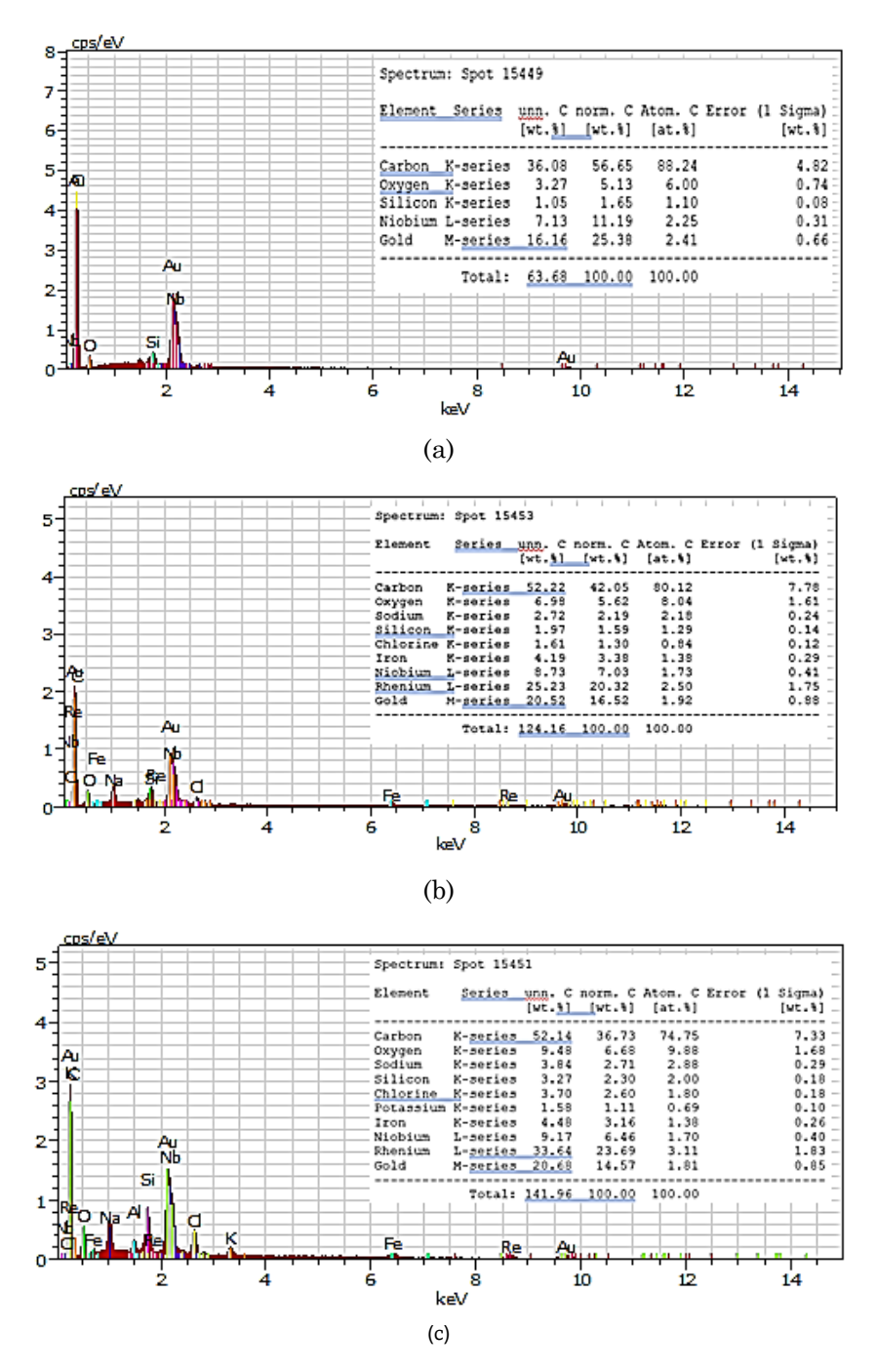


Fig 4 EDX data for (a) unmodified AC (b) 30% H<sub>2</sub>SO<sub>4</sub> + ZnCl<sub>2</sub> MAC (c) 75% H<sub>2</sub>SO<sub>4</sub> + ZnCl<sub>2</sub> MAC

steel tray used. Low potassium (K) concentration was detected in 75%  $H_2SO_4$  +  $ZnCl_2$  MAC which was due to insufficient washing step from residual potassium hydroxide deposited during the neutralization step. Besides that, the detection of chlorine elements only found in 30% and 75%  $H_2SO_4$  +  $ZnCl_2$  MAC confirmed the successful loading of  $ZnCl_2$  on the surface of AC. Minerals such as Niobium (Nb) was low after the introduction of concentrated acid. Both of the MACs showed increased oxygen content as compared to unmodified AC. This was because more oxygen was bonded to carbon after modification (Mahmud  $et\ al.$ , 2018).

# 3.5 Surface morphology analysis of MAC

Surface morphology analysis such as average Feret diameter, average pore size, surface area and porosity are important to identify the improvements made on the surface which could enhance the uptake of adsorbate molecules. The SEM images of unmodified, 30% and 75%  $\rm H_2SO_4 + ZnCl_2$  MAC at 3000x magnification were analyzed using ImageJ software. The data of average Feret diameter and average pore size was used to plot histogram (Measurement distribution) and bell curve (Normal Distribution Approximation) while the average pore size and porosity were taken directly from the software. The results of the targeted outlined object were limited to pore size more than 0.5  $\mu m^2$  and circularity more than 0.5 to remove

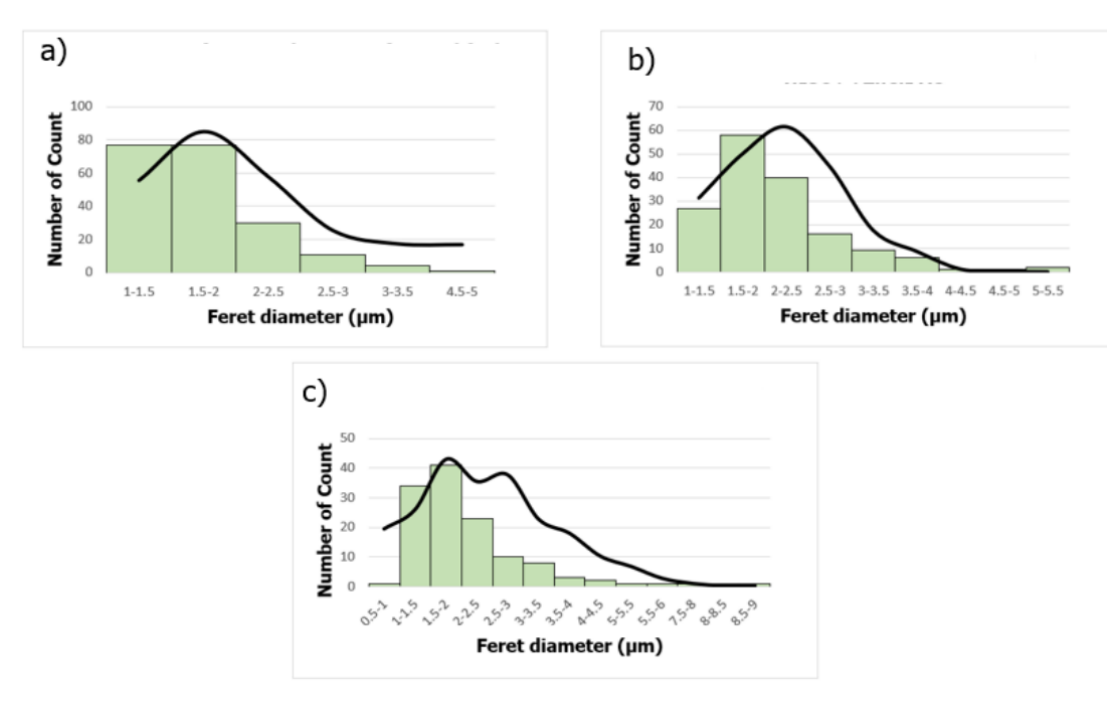


Fig 5 Pore diameter distribution for a) unmodified AC, b) 30% H<sub>2</sub>SO<sub>4</sub> + ZnCl<sub>2</sub> MAC, c) 75% H<sub>2</sub>SO<sub>4</sub> + ZnCl<sub>2</sub> MAC

unwanted objects such as cracks which are not taken into account when counting macropores. The Feret's diameter, also known as "calliper length," denotes the circumscribed circle's diameter or the largest distance between any two locations along the object's perimeter. The average Feret diameter is used to determine the pore diameter of the samples. This because the pores do not have fixed shape or size. Fig shows three pore diameter distribution of unmodified, 30% and 75%  $\rm H_2SO_4$  +  $\rm ZnCl_2$  MAC. According to the Figure 5, the average pore diameter of unmodified, 30% and 75%  $\rm H_2SO_4$  +  $\rm ZnCl_2$  modified AC are 1.765  $\rm \mu m$ , 2.105  $\rm \mu m$  and 2.137  $\rm \mu m$  respectively. Both MACs showed significant increase in pore diameter as compared to unmodified AC. The increment in pore diameter of 30% and 75%  $\rm H_2SO_4$  +  $\rm ZnCl_2$  modified AC were 19.26 and 21.08% respectively. According to the International Union of

Pure and Applied Chemistry (IUPAC), the pores identified on all of the AC samples were macropores, which gives passage of adsorbates to micropores (Alves, 2021). The increase on pore diameter on both MAC surfaces, signifies that  $\rm H_2SO_4$  and  $\rm ZnCl_2$  successfully enlarged the pores in the carbonaceous structure. Similarly, Okhovat *et al*, 2012 reported that the introduction of  $\rm ZnCl_2$  of 1:1 impregnation ratio caused the transformation of micropores into mesopores, resulting in the increased of pore diameter. Moreover,  $\rm H_2SO_4$  occupies a defined volume, preventing particle contraction during activation and generating porosity when recovered by washing following carbonization (Khalil *et al.*, 2000).

Pore size is an important parameter for adsorption of DBT, QUI and IND. Bigger pore size is essential because it indicates whether the pore is plugged, partially plugged or wide open.

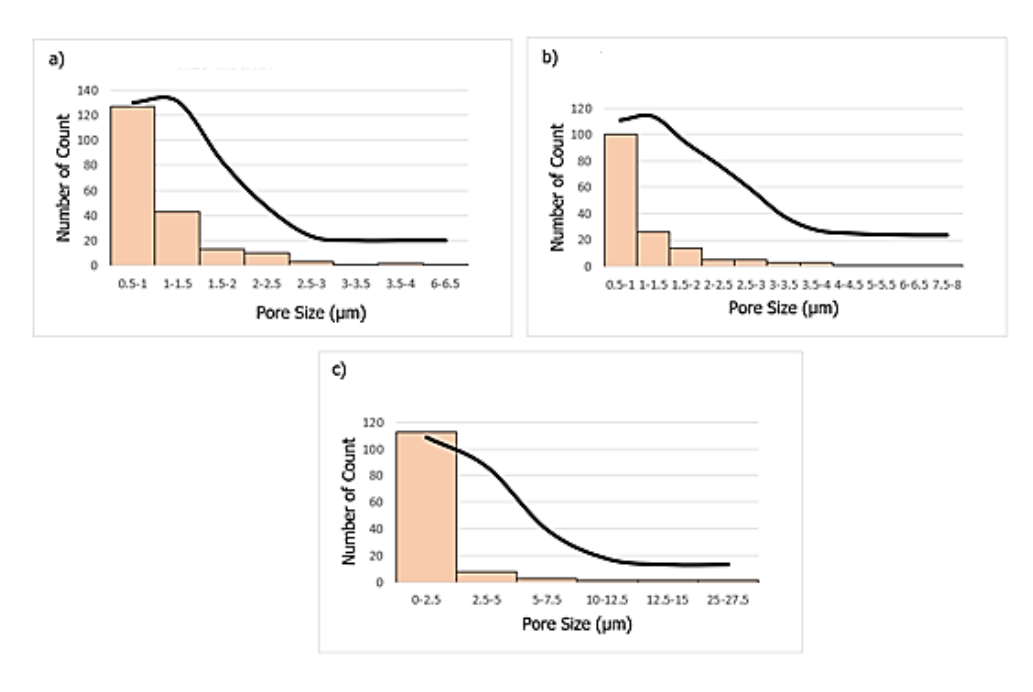


Fig. 6 Pore size distribution for a) unmodified AC, b) 30% H<sub>2</sub>SO<sub>4</sub> + ZnCl<sub>2</sub> MAC c) 75% H<sub>2</sub>SO<sub>4</sub> + ZnCl<sub>2</sub> MAC

Table 2

Pore characteristics determined using ImageJ

Type of AC	Average pore size, µm	Surface area, m <sup>2</sup> /g	Porosity, %
Unmodified	1.043	293.02	17.86
$30\% H_2SO_4 + ZnCl_2$	1.206	196.02	27.87
75% H <sub>2</sub> SO <sub>4</sub> + ZnCl <sub>2</sub>	1.546	193.28	34.09

The higher the pore size present on the surface, the better the adsorption performance of the AC since more molecules can bind on the active sites which are favorable. Fig. shows three pore size distribution of unmodified, 30% and 75% H<sub>2</sub>SO<sub>4</sub> + ZnCl<sub>2</sub> MAC. The average pore size for unmodified, 30% and  $75\% \text{ H}_2\text{SO}_4 + \text{ZnCl}_2 \text{ modified AC were } 1.043 \,\mu\text{m}, \, 1.206 \,\mu\text{m} \, \text{and}$ 1.546 µm respectively. Both MACs showed significant improvement in pore area as compared to unmodified AC. As discussed in the previous section, the pore diameter increased upon modification, thus it is also expected that the pore size will increase as well. According to past research studies, chemical activation using ZnCl2 and acids has proven to decrease the quantity of contaminants that cover pore surface, hence resulting in enlargement of pore size (Khalil et al., 2000; Okhovat et al., 2012; Yusufu et al., 2012). The enlargement of pores in this experiment are attributed to the dehydrating effect of ZnCl2 and the oxidation of carbons by H2SO4.

It is apparent from Table that both of the MAC has a higher porosity almost doubled of unmodified AC. The increase in porosity and average pore size indicates that surface area will decrease because pores are getting broader and wider. An increase in H<sub>2</sub>SO<sub>4</sub> concentration led to decreasing surface area due to the development of micropores into mesopores and macropores (Khalil *et al.*, 2000). Moreover, reduction of surface area could be due to low temperature used during modification process, hence blockage of micropores with bulky H<sub>2</sub>SO<sub>4</sub> molecule (Kolur *et al.*, 2019). In contrast, steady development of porosity occurred as H<sub>2</sub>SO<sub>4</sub> concentration increased. The higher the porosity, the greater the pores present, thus a higher availability of active sites for DBT, QUI and IND adsorption (Muhammad *et al.*, 2021).

# 3.6 Adsorption isotherm analysis

Batch experiments with constant temperature and stirring rate was conducted to identify the removal capacity of DBT in n-hexane by MAC in order to fit the data from Table 3 into respective isotherm equations as in Equations 8,10 and 11.

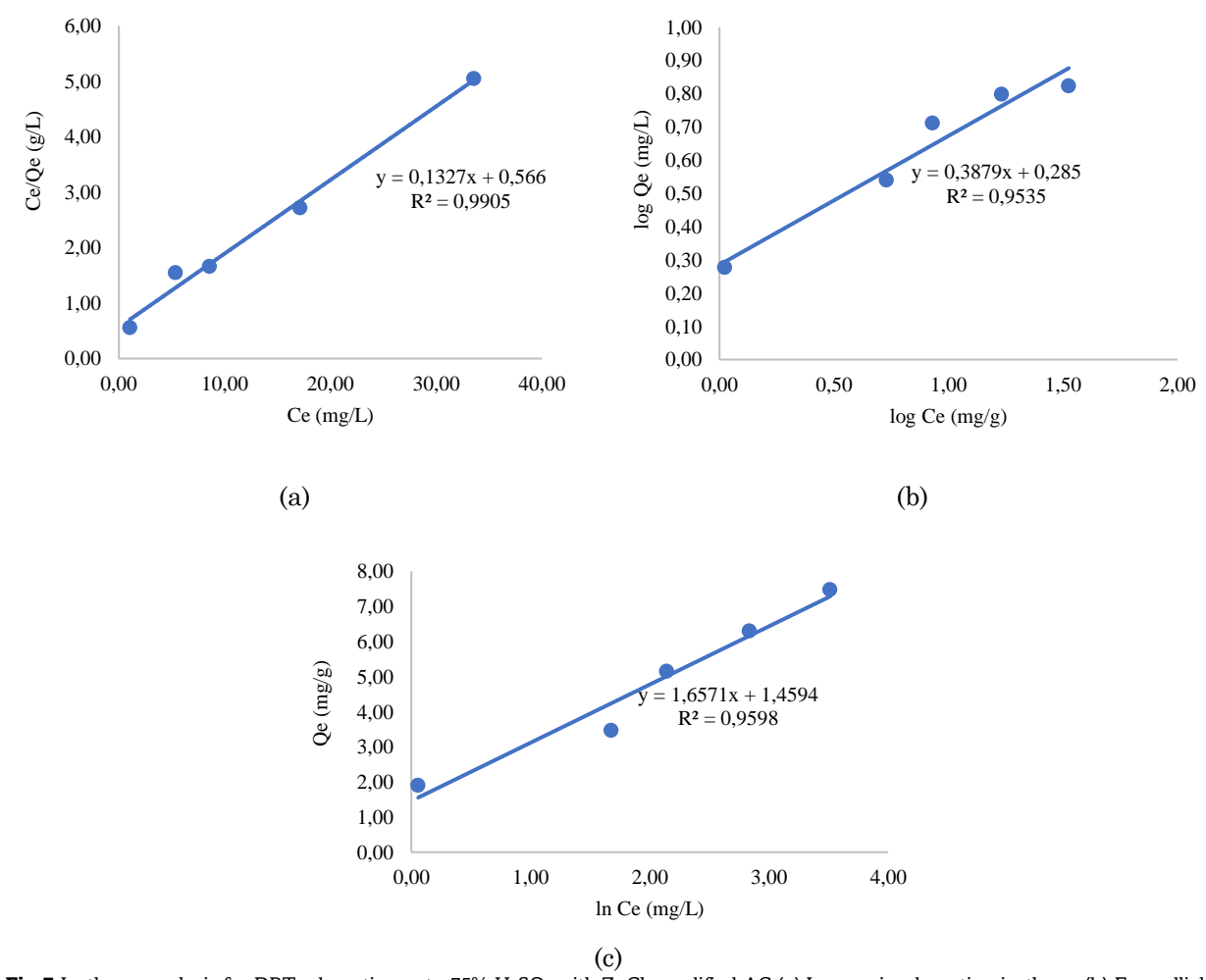
Moreover, three linear plots of Langmuir, Freundlich and Temkin for adsorptive desulphurization are shown in Figure 7. (Habeeb *et al.*, 2016; Ramutshatsha-Makhwedzha *et al.*, 2022; Sharma & Naushad, 2020). The removal capacity of QUI and IND in n-hexane by MAC was also conducted using the same procedure. Three linear plots of Langmuir, Freundlich and Temkin for adsorptive denitrogention of basic nitrogen compound, QUI, and of neutral nitrogen compound, IND was generated and shown in Figure 8 and 9.

According to the entire isotherm plot, it can be concluded that the adsorption of DBT using 75% H<sub>2</sub>SO<sub>4</sub> pre-treated AC followed by ZnCl<sub>2</sub> modification is successful. It was observed that as concentration of DBT at equilibrium increases, the adsorption capacity of DBT increases as well. This means that as initial DBT concentration an increase, adsorption performance reduces where the percentage removal range of DBT from n-hexane were in between 66.46% to 94.70%. This could be because n-hexane has hydrophobic characteristic, which is heavily absorbed by the MAC thus influencing the efficiency of DBT removal (Olajire *et al.*, 2017).

Based on the Figure 8, the entire plot shows positive increase in adsorption capacity with concentration of QUI at equilibrium. This signifies that 30% H<sub>2</sub>SO<sub>4</sub> and ZnCl<sub>2</sub> MAC is capable of reducing the concentration of QUI in n-hexane. However, it was found that as initial concentration of QUI increased, the percentage removal of QUI notably decreased ranging to be between 40.31% to 76.14% where initial concentration of QUI were 40 mg/L and 100 mg/L respectively. In this study, it can be concluded that 30% H<sub>2</sub>SO<sub>4</sub> and ZnCl2 MAC is able to effectively remove low QUI concentration in n-hexane which is between 20 mg/L to 40 mg/L. Similarly, like the adsorption of DBT onto MAC, the reduced percentage removal could be because n-hexane has hydrophobic characteristic, which was heavily absorbed by the modified AC, thus influencing the efficiency of QUI removal (Olajire et al., 2017). Moreover, the low percentage of QUI removal at higher initial concentration is due to insufficient

Table 3
Adaptation experiment data for DPT OLU and IND concentration

$C_o$ , mg/L	$C_e$ , mg/L	$Q_e$ , mg/g	percentage, %, of Removal
		DBT	
20	1.060	1.894	94.70
40	5.366	3.463	86.56
60	8.549	5.145	85.75
80	17.10	6.290	78.62
100	33.54	6.646	66.46
		QUI	
20	5.805	1.419	70.97
40	9.545	3.045	76.14
60	24.52	3.548	59.13
80	39.57	4.043	50.54
100	59.69	4.031	40.31
		IND	
20	2.386	1.761	88.07
40	13.58	2.642	66.05
60	25.51	3.449	57.49
80	43.84	3.616	45.20
100	63.91	3.609	36.09



 $\textbf{Fig 7} \ Isotherm \ analysis \ for \ DBT \ adsorption \ onto \ 75\% \ H_2SO_4 \ with \ ZnCl_2 \ modified \ AC \ (a) \ Langmuir \ adsorption \ isotherm \ (b) \ Freundlich \ adsorption \ isotherm \ (c) \ Temkin \ adsorption \ isotherm \ (d) \ Temkin \ adsorption \ isotherm \ (e) \ Temkin \ adsorption \ (e) \ Temkin \ (e) \ Tem$ 

binding sites of QUI molecule on surface of MAC since most active sites is already saturated with the QUI molecule.

All three isotherm graphs indicated increasing adsorption capacity at equilibrium when the equilibrium concentration of IND increased from 20 mg/L to 100 mg/L (Figure 9). This implies that  $75\%~H_2SO_4$  and  $ZnCl_2~MAC$  can successfully adsorb IND compounds from n-hexane. It is also observed that the removal % of IND from n-hexane declines from 88.07% to

36.09% as the equilibrium concentration increased from 20 mg/L to 100 mg/L. This suggests that the adsorption of IND is favourable at low initial concentrations of IND. This is because the ratio of IND molecules to accessible binding sites on the MAC is low, hence, indicating a higher probability of interaction between free active sites and IND molecules (Gebreslassie, 2020). On the contrary, as the number of IND molecules increases, the active site on MAC becomes saturated and is

**Table 4**Langmuir. Freundlich, and Temkin isotherm constants for adsorption of DBT, QUI and IND from n-hexane

Langmuir's Constants			
Parametrs	DBT	QUI	IND
$K_L$ , $l/mg$	0.2345	0.1104	0.2557
$Q_{max}$ ,mg/g	7.536	4.762	3.860
$R_L$	0.0427-0.2133	0.0910-0.4257	0.0391-0.1955
$R^2$	0.9905	0.9791	0.9964
Freundlich's Constants			
$K_F$ , l/mg	1.928	0.9369	0.2385
n	2.578	2.562	0.2449
$R^2$	0.9535	0.7532	0.9586
Temkin's Constants			
$A_T$ , l/mg	2.413	1.540	0.3207
$b_T$ , kJ/mol	1.496	3.019	1.588
$R^2$	0.9598	0.8410	0.9532

unable to cater to any more IND molecules, resulting in a drop percentage removal of IND. Another possible reason was the hydrophobic nature of n-hexane, which was heavily absorbed by the MAC, thus disrupting the efficiency of IND removal (Olajire *et al.*, 2017).

Table 4 shows the Langmuir, Freundlich, and Temkin isotherm constants for adsorption of DBT. OUI and IND from nhexane. The best sequence of the DBT adsorption isotherm model for this study is Langmuir > Temkin > Freundlich. As shown in Table 4, the correlation coefficient values,  $R^2$  reveals that DBT adsorption in this experimental study fits the Langmuir isotherm equation as compared to the rest since has  $R^2$ , thereby, closer to 1 ( $R^2 > 0.9905$ ). This implies that the occurrence of monolayer adsorption on limited number of homogenous active sites of 75% H<sub>2</sub>SO<sub>4</sub> pre-treated and ZnCl<sub>2</sub> MAC.  $K_L$  at 0.2345 l/mg was associated with the variation of the MAC's appropriate area and porosity, indicating that a greater surface area and pore diameter resulted in a significant adsorption capacity (Ayawei et al., 2017). The separation factor  $R_L$  indicates that the adsorption of DBT compound onto MAC was favourable and optimum since it ranged between 0 to 1. Similarly, adsorption of DBT from acid AC showed that Langmuir isotherm model was best suited for 20 to 100 mg/l

initial concentration. On the other hand, the Freundlich isotherm model had  $R^2$  closer to 1 in adsorption experiment of DBT using clay adsorbent with initial concentration ranging from 100 to 600 mg/L (Olajire et al., 2017). The value of n > 1 from Freundlich isotherm provides information that the adsorption mechanism is a reversible process, implying physisorption (Desta, 2013). The energy constant relating to enthalpy of sorption,  $b_T$  is relatively low at only 1.496 kJ/mol. Ha et al. (2019) reported a  $b_T$  value between 2715 to 4858 kJ/mol during adsorption experiment of DBT from gasoline and diesel using clay. The very low  $b_T$  value obtained in this experimental study may be attributed to the fact that DBT adsorption process using MAC involves hydrophobic interaction, which does not radiate energy as readily as ionic and polar interactions, owning to dehydration/hydration behaviour (Olajire et al., 2017).

The best sequence of the QUI adsorption isotherm model for this study was Langmuir > Temkin > Freundlich. The Langmuir adsorption isotherm model provided the best fitting to the adsorption data, since it has the highest  $R^2$  value at 0.9791

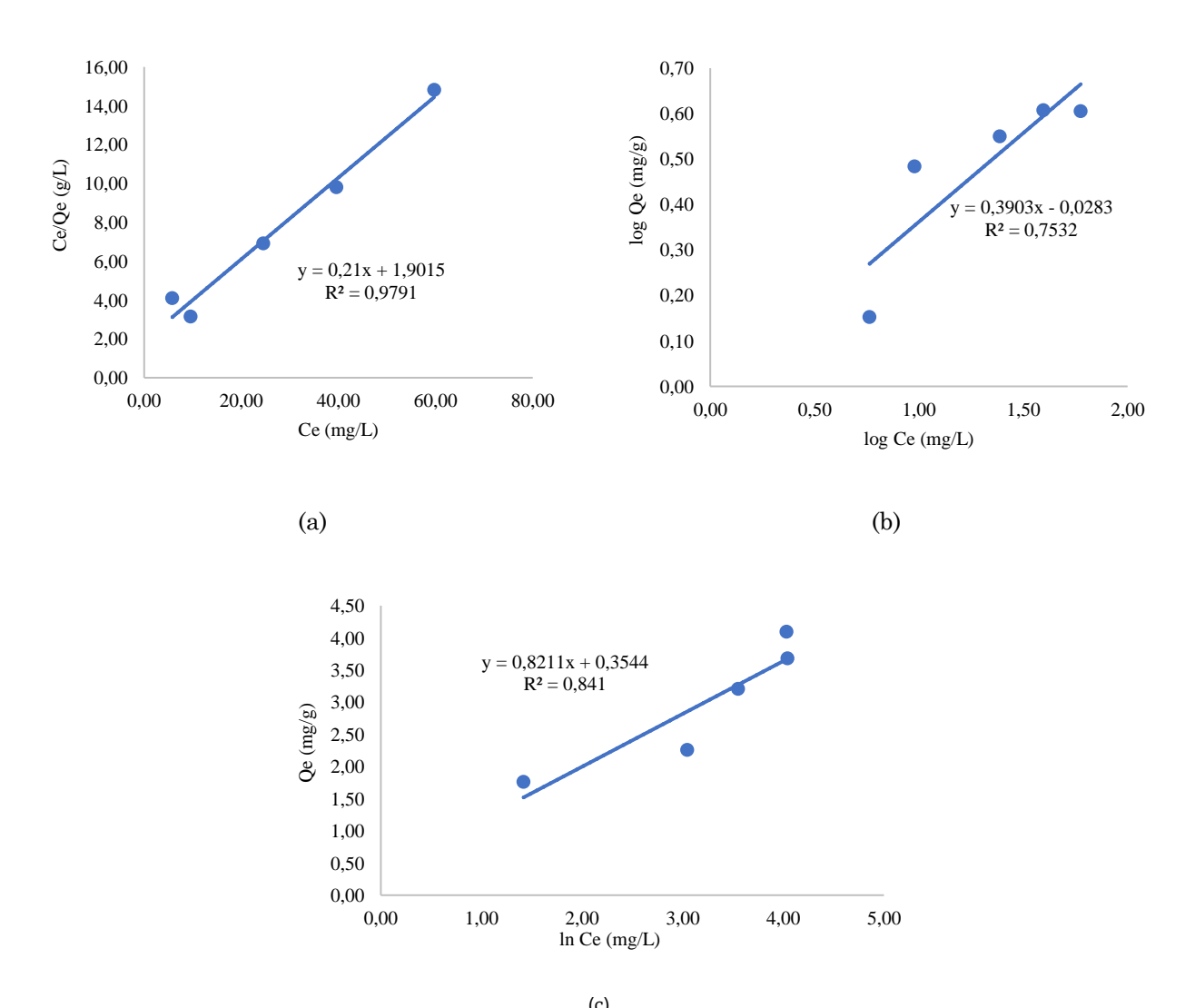


Fig 8 Isotherm analysis for QUI adsorption onto  $30\% H_2SO_4$  with  $ZnCl_2$  MAC (a) Langmuir adsorption isotherm (b) Freundlich adsorption isotherm (c) Temkin adsorption isotherm

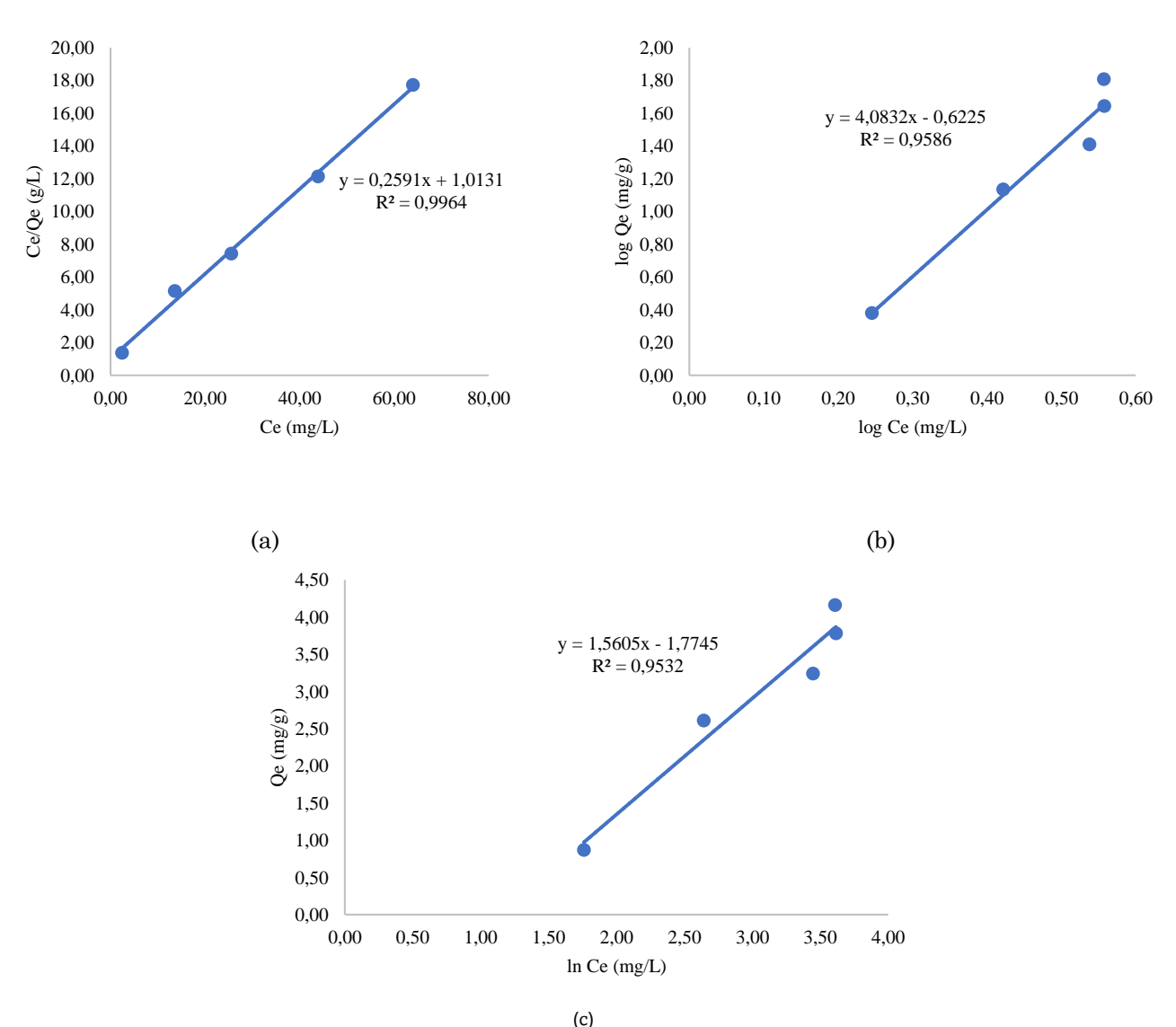


Fig 9 Isotherm analysis for IND adsorption onto 75% H<sub>2</sub>SO<sub>4</sub> with ZnCl<sub>2</sub> MAC (a) Langmuir adsorption isotherm (b) Freundlich adsorption isotherm (c) Temkin adsorption isotherm

compared to Freundlich and Temkin isotherm models. This reveals that QUI adsorption compromises entirely of a monolayer at surface of 30% H<sub>2</sub>SO<sub>4</sub> and ZnCl<sub>2</sub> MAC where only one QUI molecule can occupy a single active site. The Langmuir isotherm constant,  $K_L$  resulted to be 0.1104 l/mg which provides information on the interaction strength between QUI compound and MAC surface. The separation factor  $R_L$  shows that the adsorption of QUI compound onto modified AC is favourable and optimum since it is ranges between 0 to 1. Conversely, the correlation coefficient for Freundlich isotherm model was observed to be between 0.9486 to 0.9980 for QUI adsorption by anthracite indicating multilayer adsorption on heterogenous surface of adsorbent (Xu et al., 2019). For the QUI adsorption experiment study, it was found that n > 1 which from suggests that the adsorption mechanism of QUI is a reversible process, implying physisorption (Desta, 2013). The heat of sorption constant,  $b_T$  is relatively low at only 3.109 kJ/mol which signifies occurrence of physical and chemical adsorption of QUI on MAC. The maximum binding energy,  $A_T$  at 1.540 l/mg is quite low compared to Wang et al. (2020) research study. They reported  $A_T$  value of 5.111 l/mg during adsorption experiment of QUI from wastewater using coke powder. The Temkin adsorption isotherm model does not provide a good fit for the QUI adsorption isotherm model because liquid-phase adsorption isotherms are more complicated, however, it is suitable for gas-phase adsorption system since, particles are free-moving and do not have similar orientation (Amin *et al.*, 2015).

The best sequence of the IND adsorption isotherm model for this study slightly differs from DBT and QUI which is Langmuir > Freundlich > Temkin. Similarly, like the DBT and QUI adsorbate, the IND adsorption data is best fitted the Langmuir adsorption isotherm model, because the correlation coefficient,  $R^2$  value at 0.9964 is the closest to 1. According to Langmuir's model, the surface of 75% H<sub>2</sub>SO<sub>4</sub> and ZnCl<sub>2</sub> MAC has a specific number of binding sites, where it forms a monolayer of IND, resulting in inability of future adsorption process to take place. IND adsorption compromises entirely of a monolayer at surface of 30% H<sub>2</sub>SO<sub>4</sub> and ZnCl<sub>2</sub> MAC where only one QUI molecule can occupy a single active site. The Langmuir isotherm constant, K<sub>L</sub> which refers to energy and affinity of active site to IND compound were identified to be 0.2557 l/mg which is relatively high. Another research study by Yang et al. (2015), reported a  $K_L$  value of 0.0015 for IND adsorption by molecular imprinted polymers. However, this huge difference of values could be the differences in adsorbent

material and the surface charge on adsorbent. The separation factor,  $R_L$  shows that the adsorption of IND compound onto MAC is favourable and optimum since it is ranges between 0 to 1. Other studies have also showed that IND adsorption on various adsorbents such as molecular imprinted polymer and acid impregnated metal organic framework had a better fit to Langmuir adsorption isotherm model (Ahmed, Khan, et al., 2013; Yang et al., 2015). The value of n < 1 from Freundlich isotherm provides information that the adsorption mechanism is a irreversible process, implying chemisorption (Desta, 2013). The energy constant relating to enthalpy of sorption,  $b_T$  is relatively low at only 1.588 kJ/mol which implies physisorption and chemisorption process of IND on MAC. The heat of the sorption constant  $b_T$  is relatively low at only 1.588 kJ/mol which signifies the occurrence of physical and chemical adsorption of IND on MAC. The maximum bonding energy,  $A_T$ at 0.3207 l/mg was lower than of QUI in this research study. The Temkin model is unsuitable to describe the adsorption mechanism of IND on modified AC because it involves liquidphase adsorption process which is more complex as compared to gas-phase system (Amin et al., 2015).

### 3.7 Adsorption kinetic model analysis

Adsorption studies using two kinetic models which were the PFO and PSO were conducted to gather significant information on the chemical pathways, adsorption rate, and as well as its mechanism of adsorbates onto MAC. These observations were required to determine the effectiveness of MAC and to ascertain the best operating parameters for the maximum percentage removal of adsorbates. To identify the most suitable adsorption kinetic model, 5 batch experiments were carried out with an initial DBT concentration of 100 mg/L at constant stirring speed and temperature but with various stirring times from 1 to 5 h. The data obtained from the experiments as in Table 5 were fit into PFO model and PSO model using Equations 13 and 14. For every batch adsorption experiment of QUI and IND also followed similar methods. Then, two linear graphs were plotted for adsorptive desulphurization of DBT, QUI and IND as illustrated in Figures 10, 11 and 12.

The DBT data for this adsorption experiment using 75% H<sub>2</sub>SO<sub>4</sub> and ZnCl<sub>2</sub> MAC as shown in Table 5 demonstrates that the rate of DBT adsorption was very rapid from 0 to 1 hour, which was attributed to the existence of a significant number of vacant binding site which are accessible to the DBT molecule. However, after 1 hour, the removal % of DBT increases slightly

after each interval hour. This could be due to the reduction of active sites available for binding with DBT molecule. The results from this experimental study suggest that most of DBT compound is removed within the first hour. Similar results were obtained by Fayazi *et al.* (2015) during DBT adsorption experiment using magnetic AC which reported high DBT uptake rate within the first interval and then the adsorption rate reached dynamic equilibrium.

As shown in Table 5, as the stirring time increases, the concentration of QUI remained in n-hexane reduced almost half from the initial QUI concentration. Not only that, the removal percentage of QUI from n-hexane using 30% H<sub>2</sub>SO<sub>4</sub> and ZnCl<sub>2</sub> MAC increased over time. The rate of adsorption was relatively high for the first hour and then increased slightly after each interval to reach 45.35%. The slight increase could be due to fewer binding sites available and the repulsive forces between QUI molecule in solution as well as on modified AC surface. Similar observation on high QUI removal percentage from adsorbent within the first interval were also observed by another researcher (Xu et al., 2019). From Table 5, it can be concluded that the concentration of IND left in n-hexane decreases with as stirring time increases. This means that more IND molecule was adsorbed onto 75% H2SO4 and ZnCl2 MAC with respect to stirring time. Besides that, it can be observed from the table that as time increases, the removal percentage of IND from n-hexane using MAC increases as well. However, the removal percentage of IND is lower than of QUI because IND has higher nitrogen content; hence more nitrogen molecules need to compete for limited number of active sites on the MAC. In this study, the rate of adsorption of IND onto MAC observed high response for the first hour and then slight increment subsequently. This signifies that within the first hour, there are numerous accessible active sites for the binding of IND molecule, but after that, the remaining free IND molecule had to lesser binding sites available due to the MAC surface being saturated with bonded IND molecule. Table 6 shows the PFO and PSO constants for adsorption of DBT, QUI and IND from n-hexane

According to the data in Table 6, the adsorption of DBT from n-hexane using 75%  $\rm H_2SO_4$  and  $\rm ZnCl_2$  MAC fit perfectly into the PSO kinetic model, since it has a higher correlation coefficient,  $R^2$  at 0.9992 which is relatively close to 1 and is linear. This reveals that the chemical interaction between functional groups presents on MAC surface and DBT molecule are a rate determining step (Nazal *et al.*, 2019; Olajire *et al.*, 2017). Moreover, the calculated adsorption capacity, ( $Q_e$  (calc.) value is quite close to the experimental adsorption capacity

Advertise kinetic data for DPT OUL and IND concentration

Stirring time, hr	$C_t$ , mg/L	$Q_t$ , mg/g	Removal percentage, %
		DBT	
1	33.54	6.646	66.46
2	31.92	6.809	68.09
3	30.38	6.962	69.62
4	28.32	7.168	71.68
5	27.81	7.219	72.19
		QUI	
1	59.69	4.031	40.31
2	58.08	4.192	41.92
3	56.38	4.362	43.62
4	55.48	4.452	44.52
5	54.65	4.535	45.35
		IND	
1	63.91	3.609	36.09
2	63.82	3.618	36.18
3	63.56	6.644	36.44
4	63.16	3.684	36.84
5	62.82	3.718	37.18

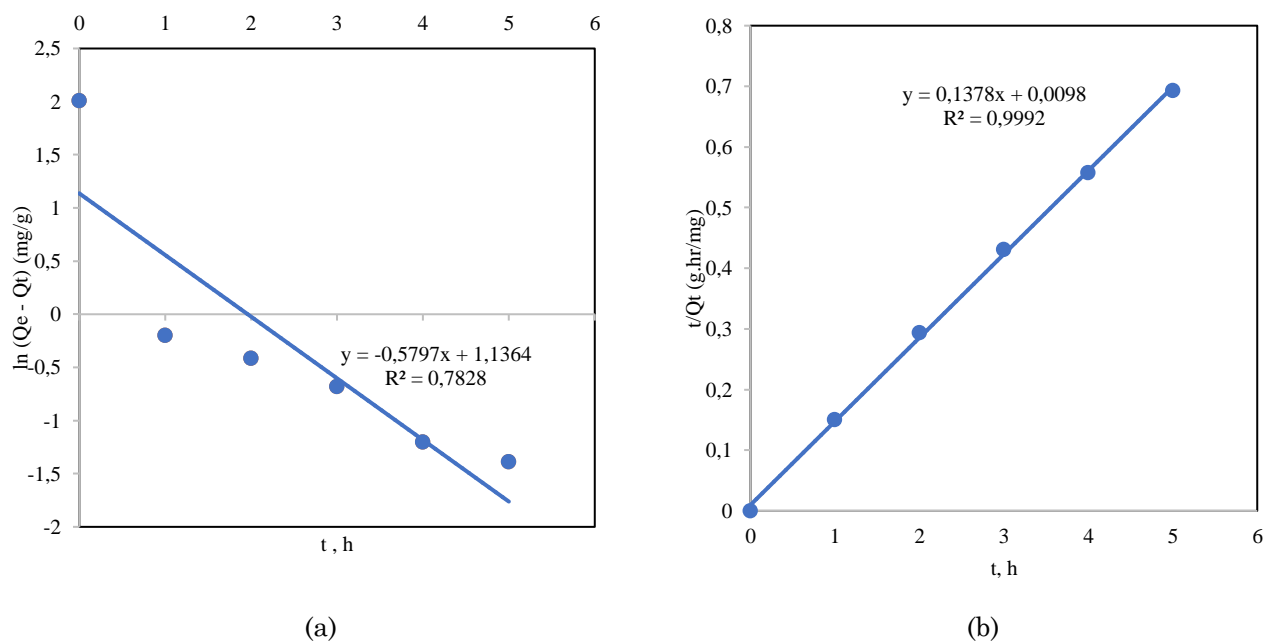


Fig 10 Kinetic model analysis for DBT adsorption onto 75% H<sub>2</sub>SO<sub>4</sub> with ZnCl<sub>2</sub> MAC (a) PFO model (b) PSO model

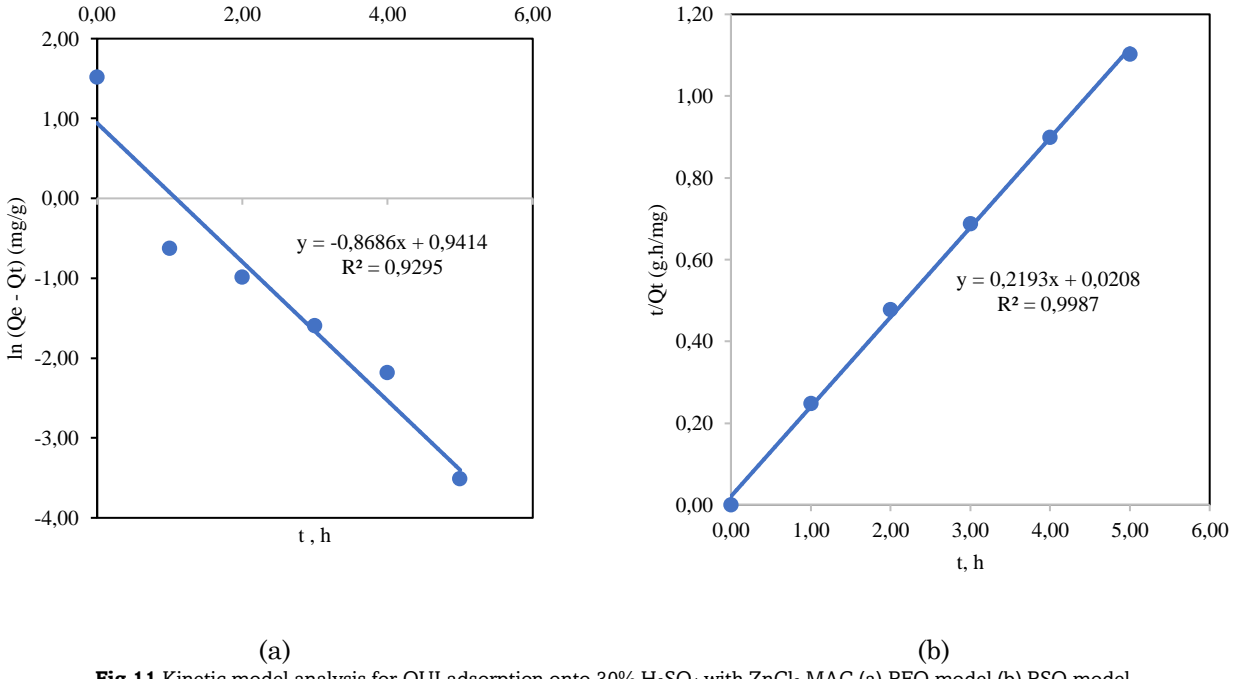


Fig 11 Kinetic model analysis for QUI adsorption onto 30% H<sub>2</sub>SO<sub>4</sub> with ZnCl<sub>2</sub> MAC (a) PFO model (b) PSO model

 $(Q_{e(\exp)})$  for PFO kinetic model as compared to PSO model. Adding to that, the difference between experimented and calculated adsorption capacity from PSO kinetic model has a percentage error of 58.28%. The kinetic rate, K2 from PSO kinetic model is also higher that than of  $K_1$  in PFO model which means that the adsorption rate of DBT onto modified AC is comparatively faster. It is also discovered that PFO kinetic model has  $\mathbb{R}^2$  of 0.7828, hence indicating that the adsorption mechanism is not appropriate to be described using PFO kinetic model. The poor R2 value for PFO kinetic model obtained from the adsorption of DBT onto modified AC had also been reported

previously by several research studies (Fayazi et al., 2015; Thaligari et al., 2018). They concluded that DBT adsorption provided a better fitting to PSO kinetic model relative to the PFO kinetic model. As listed in Table 6, for adsorption of QUI, the R2 values obtained from PFO and PSO kinetic model are well above 0.90. However, the PSO kinetic model is best to describe the adsorption mechanism of QUI from n-hexane as it has a  $R^2$  value closer to unity. The results indicated that the adsorption process of QUI onto MAC belongs to chemisorption process (Xu et al., 2019). In addition to that, the difference between the calculated adsorption capacity, (Qe(calc)) was very low to the experimental adsorption capacity (Qe(exp)) for PSO

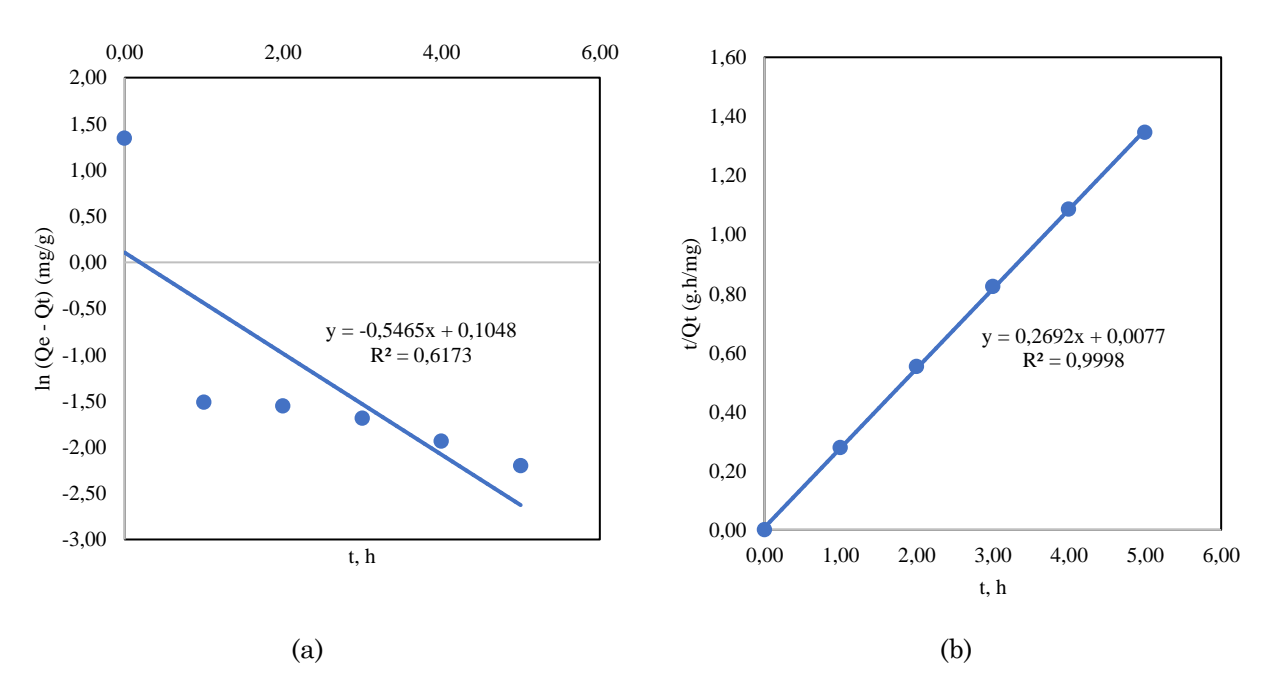


Fig 12 Kinetic model analysis for IND adsorption onto 75% H<sub>2</sub>SO<sub>4</sub> with ZnCl<sub>2</sub> MAC (a) PFO model (b) PSO model

**Table 6**Pseudo first and second order constants for adsorption of DBT, QUI and IN

		PFO constants	
Parameters	DBT	QUI	IND
$K_1$ , hr <sup>-1</sup>	0.5797	0.8686	0.5465
$Q_{e \text{ (exp)}}$ , mg/g	7.468	4.565	3.828
$Q_{e \text{ (calc)}}$ , mg/g	3.116	2.564	1.111
$R^2$	0.7828	0.9295	0.6173
		PSO constants	
$K_2$ , g/mg.hr	1.938	2.312	9.412
$Q_{e \text{ (exp)}}$ , mg/g	7.468	4.565	3.828
$Q_{e \text{ (calc)}}$ , mg/g	7.257	4.560	3.718
$R^2$	0.9992	0.9987	0.9998

kinetic model with only 0.11% error. The ( $Q_{e \text{ (calc)}}$ ) was much lower than the ( $Q_{e \text{ (exp)}}$ ) for PFO kinetic model, hence indicating that this kinetic model was unsuitable. The kinetic rate ,  $K_2$ , from PSO kinetic model was also higher that than of  $K_1$  in PFO model which means that the adsorption rate of QUI onto modified AC is relatively higher.

The results obtained during this adsorption experiment were similar to the results reported by numerous authors. Xu et al. (2019) described the removal of QUI from wastewater using anthracite and concluded that the kinetic data best fitted the PSO expression. Thaligari et al. (2018) also concluded that the PSO kinetic model best described the adsorption of QUI from iso-octane onto nickel-impregnated granular AC. Adding to that, a study conducted by Wang et al. (2020) on the adsorption of aqueous QUI solution by ion-impregnated coke powder deduced that the kinetic data provided the best fit to PSO kinetic model. Alves (2021) studied the adsorption of QUI from ethanol onto activated biochar which followed the PSO kinetic model as well. From Table 6, it can be concluded that the adsorption of IND from n-hexane using 75% H2SO4 and ZnCl2 MAC has a better fitting to the PSO kinetic model since the correlation coefficient, R2 was closer to 1 (>0.99) as compared to PFO kinetic model. Therefore, this implies that the chemisorption influenced the adsorption mechanism of IND

from n-hexane (Sahoo & Prelot, 2020). The R2 values obtained from the PFO kinetic model were below 0.99, hence this verified that PFO was inappropriate to describe the adsorption mechanism. Moreover, the calculated adsorption capacity, ( $Q_e$ (calc)) for the PFO kinetic model had a huge difference with the experimental adsorption capacity ( $Q_{e}$  (exp)), differing up to 70. 98%. Meanwhile, the PFO kinetic model presented smaller discrepancies between  $Q_{e \text{ (calc)}}$  and  $Q_{e(exp)}$ . The kinetic rate,  $K_2$ , from the PSO kinetic model was also much higher that than of  $K_1$  in PFO model which means that the adsorption rate of IND onto MAC was relatively higher. The adsorption performance of IND using molecular imprinted polymer also suggested a better fitting to the PSO kinetic model instead of the PFO kinetic model (Yang et al., 2015). Similarly, the PSO kinetic model was a better fit do the IND adsorption data reported by Hiwarkar et al. (2015), who studied the adsorption IND using bagasse fly ash and granular AC.

# 4. Conclusions

This work proved that double impregnation using  $H_2SO_4$  followed by  $ZnCl_2$  significantly increased the percentage removal of DBT, QUI, and IND as compared to raw AC. DBT and IND showed high percentage removal up to 86.23% and 82.77% respectively using 75%  $H_2SO_4$  with  $ZnCl_2$  MAC.

Meanwhile, OUI favoured 30% H<sub>2</sub>SO<sub>4</sub> with ZnCl<sub>2</sub> MAC with a % removal of 33.17% which is still higher than unmodified AC. Characterization studies including percentage yield, pH, bulk density, moisture content, ash content, and iodine number were also conducted. From these characterization tests, it was observed that a high percentage yield was obtained which is 72.08% and 71.13% for 30% and 75% H<sub>2</sub>SO<sub>4</sub> and ZnCl<sub>2</sub> MAC, respectively. The pH tested was also within the acidic range of 6 even after washing steps. Bulk densities were also favourable while the moisture and ash content were within acceptable limits. The iodine number test showed that the MAC achieved high porosity and good adsorption performance. In addition, the FTIR spectra of MAC revealed that H2SO4 was successfully introduced since there are the presence of S-H thiol and free O-H group only after the modification step. The empirical adsorption relationship between MAC, adsorbate molecules, and adsorption mechanism at equilibrium was described using Langmuir, Freundlich, and Temkin isotherm models. It was concluded that DBT, QUI, and IND followed the Langmuir isotherm model better with a correlation coefficient,  $R^2$  of 0.9905, 0.9791, and 0.9964 respectively. Moreover, the adsorption kinetic data of DBT, QUI, and IND provided a better fitting to the PSO kinetic model with  $R^2$  of 0.9992, 0.9987, and 0.9998 respectively.

### Acknowledgements

This research was supported by the Research Management Center of Universiti Malaysia Sabah (Grant No. DN21100 - Phase 1/2021). These contributions are gratefully acknowledged.

**Conflicts of Interest:** The authors declare no conflicts of interest to report regarding the present study.

# References

- Achaw, O. W. (2012) A study of the porosity of activated carbons using the scanning electron microscope. *Scanning Electron Microscopy, InTech.* http://dx.doi.org/10.5772/36337
- Ahmed, I., Hasan, Z., Khan, N. A., & Jhung, S. H. (2013). Adsorptive denitrogenation of model fuels with porous metal-organic frameworks (MOFs): Effect of acidity and basicity of MOFs. Applied Catalysis B: Environmental, 129, 123-129. https://doi.org/10.1016/j.apcatb.2012.09.020
- Akpa, J. G., & Dagde, K. K., (2018). Effect of activation method and agent on the characterization of prewinkle shell activated carbon. Chemical and Process Engineering Research, 56, 24-36. https://www.iiste.org/Journals/index.php/CPER/article/view/ 41379/42608
- Almarri, M., Ma, X., & Song, C. (2009). Selective adsorption for removal of nitrogen compounds from liquid hydrocarbon streams over carbon- and alumina-based adsorbents. *Industrial and Engineering Chemistry Research*, 48(2), 951-960. https://doi.org/10.1021/ie801010w
- Alves, G. G. (2019). Removal of quinoline from oily wastewater using biochars prepared from compost. M. Sc. Thesis, Chemical Engineering, School of Technology and Management Polytechnic Institute of Bragança. https://bibliotecadigital.ipb.pt/bitstream/10198/24011/1/Alves Giovanna.pdf
- Amin, M. T., Alazba, A. A., & Shafiq, M. (2015). Adsorptive removal of reactive black 5 from wastewater using bentonite clay: Isotherms, kinetics and thermodynamics. *Sustainability*), 7(11), 15302-15318. https://doi.org/10.3390/su71115302
- Angin, D. (2014). Production and characterization of activated carbon from sour cherry stones by zinc chloride. *Fuel*, 115, 804-811. https://doi.org/10.1016/j.fuel.2013.04.060
- Anisuzzaman, S. M., & Kamarulzaman, S. (2021). Removal of nitrogen containing compounds from fuel using modified activated carbon.

- *Transactions on Science and Technology,* 8(1), 38-44. https://tost.unise.org/pdfs/vol8/no1/ToST-8x1x38-44xOA.html
- Awe, A. A., Opeolu, B. O., Fatoki, O. S., Ayanda, O. S., Jackson, V. A., & Snyman, R. (2020). Preparation and characterisation of activated carbon from *Vitis vinifera* leaf litter and its adsorption performance for aqueous phenanthrene. *Applied Biological Chemistry*, 63(1). 1-17. https://doi.org/10.1186/s13765-020-00494-1
- Ayawei, N., Ebelegi, A. N., & Wankasi, D. (2017). Modelling and interpretation of adsorption isotherms. *Journal of Chemistry*, 2017 (3039817), 1-11. https://doi.org/10.1155/2017/3039817
- Bouchemal, N., Belhachemi, M., Merzougui, Z., & Addoun, F. (2009). The effect of temperature and impregnation ratio on the active carbon porosity. *Desalination and Water Treatment*, 10, 115-120. https://doi.org/10.5004/dwt.2009.828
- Chilev, C. (2017) A New Procedure for Porous Material Characterization. *International Journal of Science, Technology and Society*, 5(4), 131. https://doi.org/10.11648/j.ijsts.20170504.22
- Dagde, K. K. (2018) Biosorption of crude oil spill using groundnut husks and plantain peels as adsorbents. *Advances in Chemical Engineering and Science*, **8**, 161-175. https://www.scirp.org/journal/paperinformation.aspx?paperid=86190
- Dehghan, R., & Anbia, M. (2017). Zeolites for adsorptive desulfurization from fuels: A review. Fuel Processing Technology, 167, 99-116. https://www.sciencedirect.com/science/article/abs/pii/S03783 82017301637
- Desta, M. B. (2013). Batch sorption experiments: Langmuir and freundlich isotherm studies for the adsorption of textile metal ions onto teff straw (*Eragrostis tef*) agricultural waste. *Journal of Thermodynamics*, 2013 (375830), 1-6. https://doi.org/10.1155/2013/375830
- Efeovbokhan, V. E., Alagbe, E. E., Odika, B., Babalola, R., Oladimeji, T. E., Abatan, O. G., & Yusuf, E. O. (2019). Preparation and characterization of activated carbon from plantain peel and coconut shell using biological activators. *Journal of Physics: Conference Series*, 1378(3), 1-14. https://doi.org/10.1088/1742-6596/1378/3/032035
- Fayazi, M., Taher, M. A., Afzali, D., & Mostafavi, A. (2015). Removal of dibenzothiophene using activated carbon/γ-Fe2O3 nanocomposite: Kinetic and thermodynamic investigation of the removal process. *Analytical and Bioanalytical Chemistry Research*, 2(2), 73-84. https://doi.org/10.22036/abcr.2015.10158
- Gebreslassie, Y. T. (2020). Equilibrium, kinetics, and thermodynamic studies of malachite green adsorption onto fig (Ficus cartia) leaves. *Journal of Analytical Methods in Chemistry*, 2020(7384675), 1-11. https://doi.org/10.1155/2020/7384675
- Ha, J. W., Japhe, T., Demeke, T., Moreno, B., & Navarro, A. E. (2019). On the removal and desorption of sulfur compounds from model fuels with modified clays. *Clean Technologies*, 1(1), 58-69. https://doi.org/10.3390/cleantechnol1010005
- Habeeb, O. A., Ramesh, K., Ali, G. A., Yunus, R. M., Thanusha, T. K., & Olalere, O. A. (2016). Modeling and optimization for H<sub>2</sub>S adsorption from wastewater using coconut shell based activated carbon. *Australian Journal of Basic and Applied Science*, 10(17), 136-147. http://umpir.ump.edu.my/id/eprint/17298/1/fkksa-2016-ramesh-Modeling%20and%20Optimization%20for%20H2S.pdf
- Hakimi M. S. M. S. Zaini, M. A. A., & Nasri, N. S. (2017). Isotherm studies of methylene blue adsorption onto waste tyre pyrolysis powder-based activated carbons Article history. *Malaysian Journal of Fundamental and Applied Sciences*, 13(4). 671-675. https://www.researchgate.net/publication/324407270\_Isotherm\_studies\_of\_methylene\_blue\_adsorption\_onto\_waste\_tyre\_pyrolysis\_powder-based\_activated\_carbons
- Hiwarkar, A. D, Srivastava, V. C., & Mall I. D. (2015). Comparative studies on adsorptive removal of indole by granular activated carbon and bagasse fly ash. *Environmental Progress & Sustainable Energy*, 34(2), 492–503. https://doi.org/10.1002/ep.12025
- Iwanow, M., Gärtner, T., Sieber, V., & König, B. (2020). Activated carbon as catalyst support: Precursors, preparation, modification and characterization. *Beilstein Journal of Organic Chemistry*, 16, 1188-1202. https://www.beilstein-journals.org/bjoc/articles/16/104
- Jawad, A. H., Rashid, R. A., Ishak, M. A. M., & Wilson, L. D. (2016). Adsorption of methylene blue onto activated carbon developed from biomass waste by H<sub>2</sub>SO<sub>4</sub> activation: kinetic, equilibrium and

- thermodynamic studies. *Desalination and Water Treatment*, 57(52), 25194-25206. https://doi.org/10.1080/19443994.2016.1144534
- Jeyakumar, R. P. S., & Chandrasekaran, V. (2014). Preparation and characterization of activated carbons derived from marine green algae *Ulva fasciata sp. Asian Journal of Chemistry*, 26(9), 2545-2549. https://doi.org/10.14233/ajchem.2014.15723
- Khalil, L. B., Girgis, B. S., & Tawfik, T. A. M. (2000). Porosity characteristics of activated carbons derived from olive oil wastes impregnated with H<sub>3</sub>PO<sub>4</sub>. Adsorption Science & Technology, 18(4), 373-383.
  - https://journals.sagepub.com/doi/pdf/10.1260/0263617001493
- Kolur, N. A., Sharifian, S., & Kaghazchi, T. (2019). Investigation of sulfuric acid-treated activated carbon properties. *Turkish Journal* of Chemistry, 43(2), 663–675. https://doi.org/10.3906/kim-1810-63
- Lee, S. H. D., Kumar, R., & Krumpelt, M. (2002). Sulfur removal from diesel fuel-contaminated methanol. In *Separation and Purification Technology*, 26(2-3), 247-258. https://www.sciencedirect.com/science/article/abs/pii/S13835 86601001745
- Lesaoana, M., Mlaba, R. P. V., Mtunzi, F. M., Klink, M. J., Edijike, P., & Pakade, V. E. (2019). Influence of inorganic acid modification on Cr(VI) adsorption performance and the physicochemical properties of activated carbon. South African Journal of Chemical Engineering 28, 8-18. https://www.sciencedirect.com/science/article/pii/S1026918518300222?via%3Dihub
- Lopes, A. R., Scheer, A. de P., Silva, G. V., & Yamamoto, C. I. (2016). Pd-Impregnated activated carbon and treatment acid to remove sulfur and nitrogen from diesel. *Matéria (Rio de Janeiro)*, 21(2), 407-415. https://doi.org/10.1590/S1517-707620160002.0038
- Mahmud, N. A., Osman, N., & Jani, A. M. M. (2018). Characterization of acid treated activated carbon from oil palm empty fruit bunches (EFB). *Journal of Physics: Conference Series*, 1083, 1-6. https://doi.org/10.1088/1742-6596/1083/1/012049
- Martínez-Mendoza, K. L., Barraza Burgos, J. M., Marriaga-Cabrales, N., Machuca-Martinez, F., Barajas, M. and Romero, M. (2020). Production and characterization of activated carbon from coal for gold adsorption in cyanide solutions. *Ingenieria e Investigación*, 40(1), 34-44. https://doi.org/10.15446/ing.investig.v40n1.80126
- Mkungunugwa, T., Manhokwe, S., Chawafambira, A., & Shumba, M. (2021). Synthesis and characterisation of activated carbon obtained from marula (Sclerocarya birrea) nutshell. *Journal of Chemistry*, 2021, 1-9. https://doi.org/10.1155/2021/5552224
- Mopoung, S., Moonsri, P., Palas, W., & Khumpai, S. (2015). Characterization and properties of activated carbon prepared from tamarind seeds by KOH activation for Fe(III) adsorption from aqueous solution. *The Scientific World Journal*, 2015. 1-9. https://doi.org/10.1155/2015/415961
- Muhammad, M. U., Hadi, B. A., & Abduljalil, M. M. (2021). Preparation of high surface area activated carbon from native rice husk. *London Journal of Engineering Research*, 21(3), 13-19. https://www.researchgate.net/profile/Abduljalil-Muhammad-Mode/publication/363700327\_Preparation\_of\_High\_Surface\_Ar ea\_Activated\_Carbon\_from\_Native\_Rice\_Husk/links/632ae6ed0 71ea12e364e226c/Preparation-of-High-Surface-Area-Activated-Carbon-from-Native-Rice-Husk.pdf
- Mühlen, C. V, Oliveira, D., Zini, C. A., Caramão, E. B., & Marriott, P. J. (2010). Characterization of nitrogen-containing compounds in heavy gas oil petroleum fractions using comprehensive two-dimensional gas chromatography coupled to time-of-flight mass spectrometry. *Energy and Fuels*, 24(6), 3572-3580. https://doi.org/10.1021/ef1002364
- Nazal, M. K., Khaled, M., Atieh, M. A., Aljundi, I. H., Oweimreen, G. A., & Abulkibash, A. M. (2019). The nature and kinetics of the adsorption of dibenzothiophene in model diesel fuel on carbonaceous materials loaded with aluminum oxide particles. *Arabian Journal of Chemistry*, 12(8), 3678-3691. https://doi.org/10.1016/j.arabjc.2015.12.003
- Okhovat, A., Ahmadpour, A., Ahmadpour, F., & Yadegar, Z. K., (2012). Pore size distribution analysis of coal-based activated carbons: investigating the effects of activating agent and chemical ratio. ISRN Chemical Engineering, 2012, 1-10. https://doi.org/10.5402/2012/352574

- Olajire, A. A., Abidemi, J. J., Lateef, A., & Benson, N. U. (2017). Adsorptive desulphurization of model oil by Ag nanoparticles-modified activated carbon prepared from brewer's spent grains. *Journal of Environmental Chemical Engineering*, 5(1), 147-159. https://doi.org/10.1016/j.jece.2016.11.033
- Oliveira, F. M. E., Vaz, B. G., Borba, C. E., Alonso, C. G. & Ostroski I. C. (2019). Modified activated carbon as a promising adsorbent for quinoline removal. *Microporous and Mesoporous Materials*, 277, 208-216.
  - https://www.sciencedirect.com/science/article/abs/pii/S1387181118305675
- Owabor, C., & Iyaomolere, A. (2013). Evaluation of the influence of salt treatment on the structure of pyrolyzed periwinkle shell. *Journal of Applied Sciences and Environmental Management*, 17(2). 321-327. https://doi.org/10.4314/jasem.v17i2.15
- Pratumpong, P., & Toommee, S. (2016). Utilization of zinc chloride for surface modification of activated carbon derived from Jatropha curcas L. for absorbent material. *Data in Brief*, 9, 970-975. https://doi.org/10.1016/j.dib.2016.11.019
- Qu, D., Feng, X., Li, N., Ma, X., Shang, C., & Chen, X. D. (2016). Adsorption of heterocyclic sulfur and nitrogen compounds in liquid hydrocarbons on activated carbons modified by oxidation: Capacity, selectivity and mechanism. RSC Advances, 6(48), 41982-41990. https://doi.org/10.1039/c6ra06108g
- Ramutshatsha-Makhwedzha, D., Mavhungu, A., Moropeng, M. L., & Mbaya, R. (2022). Activated carbon derived from waste orange and lemon peels for the adsorption of methyl orange and methylene blue dyes from wastewater. *Heliyon*, 8(8), e09930. https://doi.org/10.1016/j.heliyon.2022.e09930
- Sahoo, T. R., & Prelot, B. (2020). Adsorption processes for the removal of contaminants from wastewater: the perspective role of nanomaterials and nanotechnology. *Nanomaterials for the Detection and Removal of Wastewater Pollutants, Micro and Nano Technologies*, 161-222. https://doi.org/10.1016/B978-0-12-818489-9.00007-4
- Sarker, M., An, H. J., & Jhung, S. H. (2018). Adsorptive Removal of Indole and Quinoline from Model Fuel over Various UiO-66s: Quantitative Contributions of H-Bonding and Acid-Base Interactions to Adsorption. *The Journal of Physical Chemistry C*, 122(8), 4532-4539. https://doi.org/10.1021/acs.jpcc.8b00761
- Seredych, M., Lison, J., Jans, U., & Bandosz, T. J. (2009). Textural and chemical factors affecting adsorption capacity of activated carbon in highly efficient desulfurization of diesel fuel. *Carbon*, 47(10), 2491–2500. https://doi.org/10.1016/j.carbon.2009.05.001
- Sharma, G., & Naushad, M. (2020). Adsorptive removal of noxious cadmium ions from aqueous medium using activated carbon/zirconium oxide composite: Isotherm and kinetic modelling. *Journal of Molecular Liquids*, 310, 113025. https://doi.org/10.1016/j.molliq.2020.113025
- Srivastava, V. C. (2012). An evaluation of desulfurization technologies for sulfur removal from liquid fuels. RSC Advances, 2, 759-783. https://doi.org/10.1039/c1ra00309g
- Suhdi, & Wang, S. C. (2021). Fine activated carbon from rubber fruit shell prepared by using zncl2 and koh activation. *Applied Sciences*, 11(9), 3994. https://doi.org/10.3390/app11093994
- Tan, I. A. W., Abdullah, M. O., Lim, L. L. P. & Yeo, T. H. C. 2017. Surface modification and characterization of coconut shell-based activated carbon subjected to acidic and alkaline treatments. *Journal of Applied Science & Process Engineering*, 4(2), 186-194. https://publisher.unimas.my/ojs/index.php/JASPE/article/view/435
- Thaligari, K. S., Gupta, S., Srivastava, V. C., & Prasad, B. (2018).

  Adsorptive desulfurization and denitrogenation by nickel impregnated activated carbon. *Indian Journal of Chemical Technology*, 25, 522-530.

  http://op.niscpr.res.in/index.php/IJCT/article/viewFile/16026/465464933
- Tsai, C. Y., Chiu, C. H., Chuang, M. W., & Hsi, H. C. (2017). Influences of copper(II) chloride impregnation on activated carbon for low-concentration elemental mercury adsorption from simulated coal combustion flue gas. *Aerosol and Air Quality Research*, 17(6), 1637-1648. https://doi.org/10.4209/aaqr.2016.10.0435
- Wang, L., Gao, Q., Li, Z., & Wang, Y. (2020). Improved removal of quinoline from wastewater using coke powder with inorganic ions. *Processes*, 8(2). 156. https://doi.org/10.3390/PR8020156
- Wang, Y., & Yang, R. T. (2007). Desulfurization of liquid fuels by adsorption on carbon-based sorbents and ultrasound-assisted

- 3825-3831. sorbent regeneration. Langmuir, 23(7), https://doi.org/10.1021/la063364z
- Wu, S. & Chen J. P. 2008. Modification of a commercial activated carbon for metal adsorption by several approaches. Indian Journal of Environmental Protection, 28(8), https://www.researchgate.net/publication/287574842\_Modifica  $tion\_of\_a\_commercial\_activated\_carbon\_for\_metal\_adsorption\_b$ y\_several\_approaches
- Xu, H., Sun, X., Yu, Y., Liu, G., Ma, L., & Huang, G. (2019). Removal of quinoline using various particle sizes anthracite: Adsorption kinetics and adsorption isotherms. Physicochemical Problems of Processing, 55(1), 196-207. https://doi.org/10.5277/ppmp18121
- Yahya, M. A., Al-Qodah, Z., & Ngah, C. W. Z. (2015). Agricultural biowaste materials as potential sustainable precursors used for activated carbon production: A review. Renewable and Sustainable Reviews, 46, https://doi.org/10.1016/j.rser.2015.02.051
- Yakub, I., Mohammad, M., & Yaakob, Z. (2013). Effects of zinc chloride impregnation on the characteristics of activated carbon produced from physic nut seed hull. Advanced Materials Research, 626, 751-755. https://doi.org/10.4028/www.scientific.net/AMR.626.751

- Yang, W., Cao, Y., Ni, X., Hunag, W., & Xu, W. (2015). Synthesis of a Denitrification Adsorbent with Large Surface Area and Specific Pore Structure for the Removal of Indole from Fuel Oil. Adsorption and Technology, 33(5):441-456. Science https://journals.sagepub.com/doi/pdf/10.1260/0263-6174.33.5.441
- Yusufu M. I. Ariahu, C. C., & Igbabul, B. D. (2012). Production and characterization of activated carbon from selected local raw materials. African Journal of Pure and Applied Chemistry, 6(9). 123
  - http://www.academicjournals.org/app/webroot/article/article1 381242825\_Yusufu%20et%20al.pdf
- Zhou, L., Li, M., Sun, Y., & Zhou, Y. (2001). Effect of moisture in microporous activated carbon on the adsorption of methane. 39, https://www.researchgate.net/publication/244317580\_Effect\_of \_moisture\_in\_microporous\_activated\_carbon\_on\_the\_adsorption of\_methane
- Zulkania, A., Hanum, G. F., & Rezki, A. S. (2018). The potential of activated carbon derived from bio-char waste of bio-oil pyrolysis as adsorbent. MATEC Web of Conferences, 154, 1-6. https://doi.org/10.1051/matecconf/201815401029



© 2024. The author (s). This article is an open-access article distributed under the Attribution-ShareAlike 4.0 (CC BY-SA) International License (http://creativecommons.org/licenses/by-sa/4.0/) © 2024. The author (s). This article is an open-access article distributed under the terms and conditions of the Creative Commons